3-2020

Conduction Mapping for Quality Control of Laser Powder Bed Fusion Additive Manufacturing

Chance M. Baxter

Conduction Mapping for Quality Control of Laser Powder Bed Fusion Additive Manufacturing

THESIS

Chance Baxter, Second Lieutenant, USAF

AFIT-ENP-MS-20-M-080

DEPARTMENT OF THE AIR FORCE
AIR UNIVERSITY

AIR FORCE INSTITUTE OF TECHNOLOGY

Wright-Patterson Air Force Base, Ohio

AFIT-ENP-MS-20-M-080

CONDUCTION MAPPING FOR QUALITY CONTROL OF LASER POWDER BED FUSION ADDITIVE MANUFACTURING

THESIS

Presented to the Faculty

Department of Engineering Physics

Graduate School of Engineering and Management

Air Force Institute of Technology

Air University

Air Education and Training Command

in Partial Fulfillment of the Requirements for the

Degree of Master of Science in Materials Science

Chance Baxter, B.S.

Second Lieutenant, USAF

March 2020

AFIT-ENP-MS-20-M-080

CONDUCTION MAPPING FOR QUALITY CONTROL OF LASER POWDER BED FUSION ADDITIVE MANUFACTURING

Chance Baxter, B.S.
Second Lieutenant, USAF

Committee Membership:

Maj Nicholas Herr, PhD
Chairman

Maj Ryan Kemnitz, PhD
Member

Dr. Christopher Rice
Member

ADEDJI B. BADIRU, PhD
Dean, Graduate School of Engineering and Management

AFIT-ENP-MS-20-M-080

Abstract

A process was developed to identify potential defects in previous layers of Selective Laser Melting (SLM) Powder Bed Fusion (PBF) 3D printed metal parts using a mid-IR thermal camera to track infrared 3.8-4 μm band emission over time as the part cooled to ambient temperature. Efforts focused on identifying anomalies in thermal conduction. To simplify the approach and reduce the need for significant computation, no attempts were made to calibrate measured intensity, extract surface temperature, apply machine learning, or compare measured cool-down behavior to computer model predictions. Raw intensity cool-down curves were fit to a simplified functional form designed to approximate the behavior of radiative, conductive, and convective heat transfer, yielding a conductivity parameter. This parameter was able to identify minor changes, less than twenty five percent, in the thickness of a single layer of the walls of single-pass, thin-wall structures and the presence of underlying unfused powder. Small voids were not produced in the test prints analyzed here. The thermal signature of underlying fusion defects, as measured by the conductivity parameter, is clearly present for many layers. This method was shown to be effective in detecting changes in conductivity of the material which represents a large portion of the defects commonly found in SLM additive manufacturing.

Acknowledgements

Coding hurts

Thank you to my beautiful wife and our little pup for constantly providing the well needed distraction from writing this horrid document and constantly reminding me that there is more to life than school.

Thank you to everyone who has helped to edit this document. It needed it.

Thank you to the AFIT additive manufacturing lab for their support providing all necessary print materials and access to your incredible facility. Especially, thanks to Cayla Eckley for helping to perform the critical SEM analysis for this project.

Thank you to my advisor and committee chair. This project would not have come to fruition without your guidance and contributions.

Thank you to all my fellow students who struggled with me through difficult coursework and all the other challenges with completing this degree.

Thank you to everyone who has and is going to read this document. It means a lot to know that I am doing more than speaking into the void.

Chance Baxter

Table of Contents

Page

List of Figures

List of Abbreviations

CONDUCTION MAPPING FOR QUALITY CONTROL OF LASER POWDER BED FUSION ADDITIVE MANUFACTURING

I. Introduction

The demand for Additive Manufacturing (AM) from industry and defense has only risen since the advent of the technology in the early 2000s. This manufacturing process is poised to be a disruptive technological development due to capabilities unique to AM which have not been achievable by traditional manufacturing methods.

AM is the process where by building a product layer by layer, the customer can design and manufacture complex and previously unachievable structures at will. Powder-Bed Fusion (PBF) is the AM technique where a layer of metal powder is deposited and portions of the powder melted into solid parts, then the powder-bed is lowered and reset with new powder on top of the printed layer. Laser powder-bed Fusion (LPBF) is the PBF-AM process by which a laser selectively melts metal powder into solid components. The implications of LPBF-AM are numerous and diverse. LPBF-AM allows for the production of metallic components from a number of potential feed stocks including high temperature nickel based super-alloys, steels, aluminum alloys, and many more. There are a number of metal stocks which are being investigated and many needs for a metallic components can be satisfied through LPBF-AM in theory. By building layer-wise, the internal portions of the component can be built with dramatically greater complexity. Lastly, due to the separate construction of each part, the individual products can be one-off designs or have minor variations without increasing the expense significantly, allowing for rapid innovation and development cycles.

1.1 Attraction of Additive Manufacturing

The process has numerous advantages, even for parts which were previously manufactured by other methods. Some of the benefits of LPBF-AM include modular design, rapid return, onsite production, independence from the manufacturer, and the ability to construct intricate structures. The product can be redesigned between iterations trivially when dealing with AM. The part can be designed, constructed, and tested in a matter of days. Any part can be produced anywhere as long as the necessary feed stock is available. Being able to construct the part on site and on demand reduces the necessity to wait on a third party, allowing for greater independence and freedom. Finally, the last advantage which has peaked the interest of many customers in defense and industry is the construction of filigree structures which allow for lighter internal geometries for an application. There is no necessity for machining tools to be able to reach the region for it to be complexly designed as the part is being built via AM. All of these advantages have increasingly attracted the attention of customers and researchers [1].

The medical industry has extensive interest in AM. Due to its unique demands and deep pockets, a number of research groups have investigated bio-compatible metals and designs that could replace traditional medical implants. A large area of study has been in joint replacements. Modern joint replacements use mass-produced components with very little personalization to the implants used. AM allows for each replacement to be produced matching the exact needs of the patient. Additionally, AM has been investigated to produce minute holes and internal cavities as a means of producing drug delivery mechanisms that are integrated into the component and to make the replacement lighter. The drug delivery is especially helpful for antibiotics so that the flesh surrounding the replacement is locally dosed where the risk of infection is highest [2].

The Navy has recently begun to investigate AM for fleet maintenance. One benefit is for unique aging vessels where there is no active contract for replacement components. The lifespan of these vessels could be extended by producing components on demand. Additionally, currently repair crews must carry spare parts to make repairs while the ship is underway and can be stranded if a critical component unexpectedly breaks. The use of AM would allow for a crew to produce replacement components for any part that breaks as long as the feed powder stock is available. This would reduce costs dramatically in cases where the ship would otherwise require resupply and could even reduce the cargo space needed to be dedicated to commonly replaced components. The only requirement would be a printer and the necessary raw materials [3].

One field which benefits greatly from AM is research and development especially for prototype modeling and production. Creating scale models has historically required dedicated machine shops producing unique components for testing that ultimately may be used one or two times before being redesigned. LPBF-AM provides rapid production of components that can effectively run around the clock. This manufacturing method avoids any confusion on the part of the machinist as the printer will produce exactly what the computer is coded to produce. This does not completely remove the necessity for a machine shop, but it does dramatically reduce the workload and machining complexity. Additionally, this is the only way experimental designs utilizing the unique capabilities of LPBF-AM can be produced and tested. For this reason, even beyond the dedicated research of AM, LPBF printers are ideal for machine shop support of academic and research environments.

AM has been championed by the aerospace industry in recent years. This has led to a number of alloys being repurposed or developed for AM use that can survive the demanding aerospace environment. Many of these are the nickle based super-alloys

because of their prior use in welding, a mechanistically similar process to LPBF. The interest from aerospace is because, compared to other industries, they are constantly trying to make their components lighter, more complex, and smaller. The lighter, smaller, more complex assemblies are more critical in aerospace because the engineering is performed at the edge of what is possible. The slightest competitive edge can dramatically increase performance. Partially hollow components and complex internal geometry allows for many of these properties to be maximized. Creating internal supports can allow for the part to be partially hollow not unlike the bones of birds. Intricate heat exchangers can be designed which maximize the surface area of walls separating two flows without allowing them to mix. This maximization requires highly complex geometry with small channels and thin walls. The design of these heat exchangers provided much of the guidance in designing our investigation [4].

1.2 Challenges to Additive Manufacturing

Despite the unique capabilities of AM and its potential to revolutionize the manufacturing process, there are a number of challenges that limit its wide spread application. LPBF-AM printers are relatively expensive, is difficult to scale up, limited in currently available feed-stock, produces unusual and potentially detrimental microstructural anomalies, and presents additional risks not seen in other manufacturing. These challenges are some of the reasons why it has taken years for AM processes to be adopted into regular use, and even then, only in niche industries. Additionally, there are concerns that AM parts will not be produced to the same fidelity or consistency as traditionally manufactured components. There are a number of research groups seeking to tackle these challenges and major developments have been made in recent years [1].

The issue of cost is two fold. The initial startup cost is very high since the printers

are still being produced on smaller scales to satisfy the requirements of researchers and small orders from industry. As the technology progresses and becomes more common, it is expected that the per unit cost to purchase would likely decrease. This change has already occurred for plastic AM printers making them a normal household purchase. However, precision optics, high power laser, and large mechanical components are unlikely to change price quickly. Operating costs are also very expensive, the largest being the fine metal powder which is often manufactured from scrap of traditional milling. Although this could also be reduced by larger scale production, the process of producing micron level particles is time-consuming and increasingly explosive as the size reduces. Again, this process would likely be slightly cheapened by the increase in scale, but similarly has a great deal of inherent cost that cannot be avoided without significant innovation in powder production processes.

The production by AM is advantageous for unique components, but the single unit production method is a challenge for scalability. The production cost is more linear than traditional manufacturing where the cost per unit drops dramatically, often called economies of scale. The most effective way to scale AM production is to add more printers, with the cost challenges mentioned previously. This challenge could be approached through total redesign of the printer or print design to produce multiple parts, but regardless, this issue will need to be addressed [5].

The limitation of feed-stocks is one challenge that is constantly being addressed. The issue is that not all metals can be melted into solid components by LPBF due to their thermo-mechanical properties and solidification behavior. Some metals which were originally found to be effective for this treatment were welding alloys, but this greatly restricted the applications. Welding alloys were limited, but applicable due to the similarity in physical process. For welding metals, the material is added to the already solid metal components, heated to melting, and cooled to solid material

adhering to both parts. These are the same basic steps and similar conditions to in LPBF. Over time, more alloys have been developed to allow for niche applications such as bio-compatibility or thermal stability. The development of feed-stocks is challenging due to the rigorous testing needed to quantify new material's properties, so it is often done on a case by case basis when a new capability is required. Alloys for normally welded systems like traditional aircraft or automobiles exist, but more specialized alloys that are high temperature stable, bio-compatible, or otherwise unusual must be developed on a case by case basis [6].

For certain applications, LPBF can be detrimental because the micro-structure is significantly different than previous manufacturing methods. The lower layers act as nucleation sites for the solidifying metal and results in vertical columnar grain structures that affect mechanical properties. This grain structure can be recrystallized via later heat treatments if necessary to a degree, but it can also be utilized as a beneficial morphology for applications that are asymmetrical in their loading. This particular micro-structure cannot be completely avoided and does inherently restrict some applications. However as mentioned, efforts are being made to develop recrystallization procedures that change the micro-structure [7].

One of the most significant challenges to LPBF is that it is inherently dangerous mostly due to the feed-stock powder. The extremely small particles pose a significant respiratory hazard, and can rapidly oxidize and combust if exposed to an oxygen rich atmosphere. The respiratory hazard is mitigated by performing all of the maintenance and refilling of the printer wearing proper protective equipment. The combustibility is prevented by keeping the powder under an inert atmosphere during transport and printing. These dangers are different than those presented by other manufacturing methods and it requires specialized facilities to operate that limit the adoption of this

method. Ultimately, this also increases cost, but the benefit can certainly outweigh the cost.

The final major limitation on LPBF is ensuring part quality at least equivalent to existing manufactured components. This can be done in a number of ways through destructive or non-destructive analysis methods. Some of the approaches are the same or similar to assessments made on other components. However, the best means of ensuring fidelity for LPBF parts is unique to AM processes.

1.3 Ensuring Part Fidelity

Part fidelity, ensuring that the final product accurately represents the intended design, is potentially the greatest challenge to widespread implementation of LPBF-AM. There is a great deal of concern that LPBF components will not have the same reliability as traditionally manufactured components [1, 8, 9]. However, there is always a risk, regardless of the manufacturing method, that a part is produced incorrectly. For traditional manufacturing, there are generally accepted methods of quality control. Often, a statistical approach to testing is taken to detect detrimental defects efficiently and effectively. Many of the common defects in traditional manufacturing occur on the exterior of the component so that it is easily found and corrected. The statistical approach does not work as effectively because it is significantly more difficult to make excess components for destructive testing and the fact that so many parts are manufactured uniquely. Additionally, the layerwise construction of the parts allows for errors in printing to occur in the very middle of the part where they are much more difficult to detect by simple inspection. Thin walled and filigree components are particularly sensitive to this as much of the detail is on the interior of the part and small errors have more significant impacts on the overall properties when there is less material. The combination of the difficulty of detection and unpredictable impact

makes these errors detrimental to the manufacturing process and restrictive to the adoption of LPBF-AM as a standard manufacturing process.

Traditionally manufactured components undergo a number of inspection methods in order to assess their quality and some of those methods can be applied to LPBF-AM. However, some cannot. The methods that are incompatible with LPBF-AM tend to be the destructive analysis methods. These methods seek to push a representative sample of identical components to their physical limits by systematically destroying them and finding their failure points. This is highly effective for mass-produced components such as die cast or molded parts [10]. For AM, since every part is constructed individually and the risk is largely in the variation between parts and not in their similarities, developing a representative sample pool for destructive testing would be impractical and the variation could be overwhelming simply due to the natural variation between printed components. Other methods that could more likely be helpful for LPBF-AM are some of the Nondestructive Evaluation (NDE) techniques which seek to inspect a given part for defects. Some of these methods include Computed Tomography (CT), UltraSound, conductivity measurements, dye penetration and visual inspection [11]. The last two are less helpful due to their analysis only of the surface characteristics. However, the other three offer potential post-print analysis that can find internal defects and have been investigated. Though effective, these inspection techniques can still be rather wasteful as the part must be fully constructed in order to determine its quality.

Some of the other efforts to reduce the effect of part defects are the in-depth study of the printing parameters and over-engineering, often in combination with the ex-situ inspection [4]. Printing parameters including laser scanning speed, laser scanning pattern, and laser intensity can be adjusted to reduce the likelihood of certain defects. Additionally, defects can be reduced by accounting for the printing

errors in the components by adding extra layers of support to back up in the event of failure. This is costly, but can give enough redundancy to reduce the likelihood that single errors will cause the part to be rejected by some other method, such as those mentioned previously. These methods do not serve to eliminate the defects or provide some other means of defect detection that allows the part to be corrected.

An innovative means of defect detection is to leverage the layer-wise construction to our advantage. The idea is to observe the print while it is in progress and detect any variations in observable parameters that may indicate a layer has been constructed incorrectly. The goal is to observe the print in real time and have a feedback procedure that would either terminate the print upon detection of a fatal defect or better still, implement some corrective procedure. This is currently impossible [1]. The current research gap is to confront and answer these barriers to enable active monitoring of LPBF-AM.

The goal of many quality control systems which have been investigated in recent years is to achieve real time process monitoring. The delineation between monitoring and sensing is fine but critical. Monitoring requires that the component not only be observed, but that an automatic assessment of part quality be made in real time and some corrective action taken, if necessary. The challenges to real-time process monitoring are four fold. The first challenge is that many systems require accurate calibration measurements. This is especially a problem for the systems which attempt to correlate the IR measurement to temperature. Other systems require less complex, but equally limiting means of calibration such as calibrating tracking or interference patterns. The next is the large amount of data necessary to perform many of these predictive measures. There is a limitation to on-board storage of the sensor, data transfer rates to the analysis software, and the time it takes for the analysis software to appropriately process the data to extract the relevant parameter. The next challenge

is the need for a statistical method capable of coping with the natural variability in the data. This can increase the demand on the analysis software, but ideally the data can be separated or the noise predicted in such a manner to allow the computer to detect the pattern. Finally, there is no established feedback system into the printers to perform corrective action which have been produced so-far. This is a software issue as all of the printers are controlled from a computer, but it is a challenge that faces a true quality control monitoring system [1].

In order to address these barriers to active monitoring of LPBF-AM, we have developed a new method of tracking the cooling rates for thin walled structures in an effort to detect anomalous cooling that may indicate the formation of a defect. This processing bypasses the challenges of monitoring and presents a low computational overhead compared to previous methods of mathematically determining the cooling behavior. The method in question allows for rapid post processing. With some technical modifications to the camera and advances in the data transfer capabilities, this method could be used in real time.

II. Background

Over the past decade interest in 3D printing has grown rapidly with good reason. As a result, a great deal of research has been dedicated to its development and implementation on a wider scale. The meteoric rise of the early years of additive manufacturing have slowed largely due to quality concerns, among other reasons. However, effective quality control can satisfy these concerns and bring this technology further into the mainstream. Recent publications have summarized the difficulties confronting this field and demonstrated a number of potential approaches to quality control. To gain an understanding of the current status of the field, it helps to start at the beginning.

2.1 LPBF Fundamentals

Laser Powder-Bed Fusion (LPBF) is a process by which a laser is used to melt metal powder into solid metallic components. The fundamental components of the printer are the laser and its corresponding optics, the build chamber, and the powder feeding system which is comprised of a source vat and a spreading arm that deposits a consistent layer of powder. These components operate together to construct printed parts from a computer generated source file generated by slicing a solid computer model built on another machine into printable layers. A graphic showing the general design of the printer build chamber can be found below in Figure 1.

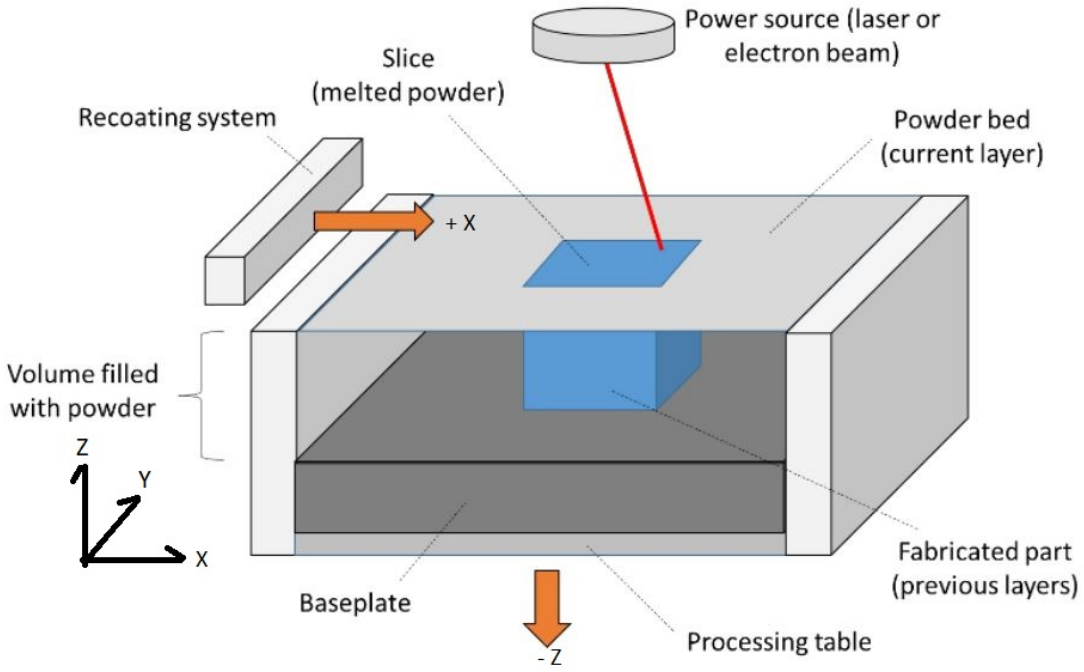

Figure 1. The 3D printer is made up of a baseplate or buildplate, the recoating system, and a laser for our case. The axes are typically labeled with the X direction pointing in the direction of the recoating arm movement and the negative Z direction pointing down into the buildplate [1].

As mentioned previously, in AM parts are constructed layer-wise. LPBF-AM machines do this through the synchronous motion of a few components. First, there is the build plate. This is a solid piece of metal on which the first layers are fused. The plate acts as a mobile stage and retreats down in the Z direction by one layer height to allow for more powder to be spread over the layer that was just printed. Next, the spreading arm deposits a set amount of powder from the powder vat over the build plate and previous layers. The arm then returns back to the starting position, leaving a consistent layer thickness and then the powder is ready for the next layer to be printed.

The process of printing each layer involves directions from the on-board computer

and the laser-optics system which steers the laser according to this design. The on-board computer follows the instructions based on the print file from the user, along with a series of build parameters, guiding the laser to melt targeted locations on the build plate using a system of optics. The speed at which the laser moves and the intensity of the beam are user defined parameters.

In addition to what laser parameters must be used, the software controlling the printer also intakes the part design from either a computer aided design software or from a fundamental code describing the laser pathway. The software then slices the design into its layer-wise 2D designs describing exactly where on each layer of build must be hit with the laser and melted. On a smaller scale, the software also controls the small level print design as one of its build parameters. For solid parts, it is not advantageous to simply raster across the whole of the print area in long rows. Instead, there are a number of small patterns which can be chosen. For example, one common design is to use a series of small hatch patterns shown in Figure 2. The shorter lines allow for the material to maintain at a higher temperature in the area of print, increasing adhesion and homogeneity across the build.

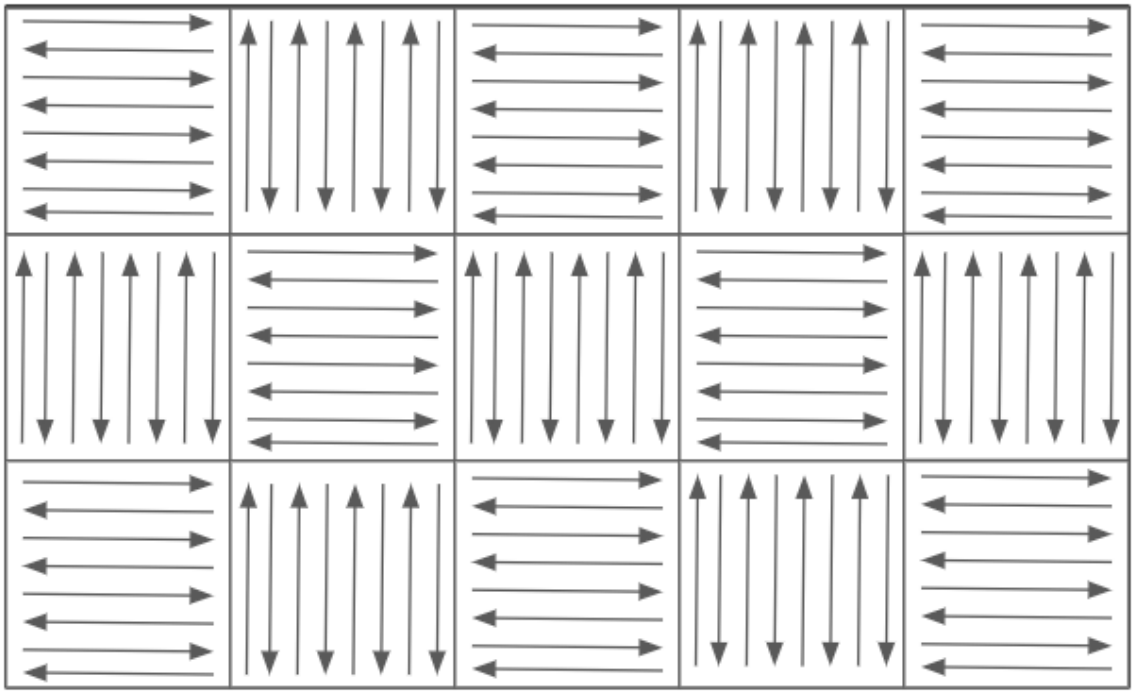

Figure 2. Printing designs such as the Hatch pattern shown here are used to achieve more homogeneous prints by reducing the thermal stress at the joining of laser tracks.

Most AM processes involve melting a feed stock and then solidifying the liquid phase onto a build plate. The process has been commercialized in recent years especially for polymers. These materials lend themselves to AM due to their relatively low melting points, for thermoplastics, or the ability to polymerize during printing, for thermosets, which can be used to achieve the liquid to solid phase transition. The thermoplastics are polymers that can be heated to melt and then cooled back to solid material. Themosets and some thermoplastics opt instead to polymerize from liquid monomers as part of the printing process typically by catalyzed reaction using ultraviolet (UV) radiation. With sufficient energetic input, metals can also be melted and re-solidified. The processes that are capable of selivering enough energy accurately are limited to Electron Bombardment Melting (EBM) and the aforementioned Selec-

tive Laser Melting. However, these methods have their drawbacks and a number of defect forming mechanisms [1].

2.2 LPBF Mechanism

The principle mechanisms involved in heating with LPBF and solidifying into solid components are radiative transfer from the Continuous Wave (CW) laser to the powder forming a localized heat source in the material and the related heat transfer away from the heated area [12]. The transfer of energy into the powder follows a Gaussian irradiance distribution of the laser (shown here is a diameter slice of the circular profile), which results in greatest transfer and highest temperature at the center of the beam Figure 3 and a penetration depth with decreasing energy deposition as the beam is absorbed in the Z direction [13]. As the powder melts and the liquid subsequently transforms into more bulk solid material the conductivity changes from the void conductivity toward the solid material conductivity. This conductivity dictates the long term cooling behavior. The heated zone then dissipates the heat in the X and Y directions into the powder as well as predominantly in the Z direction through solid connections with the underlying build material once formed.

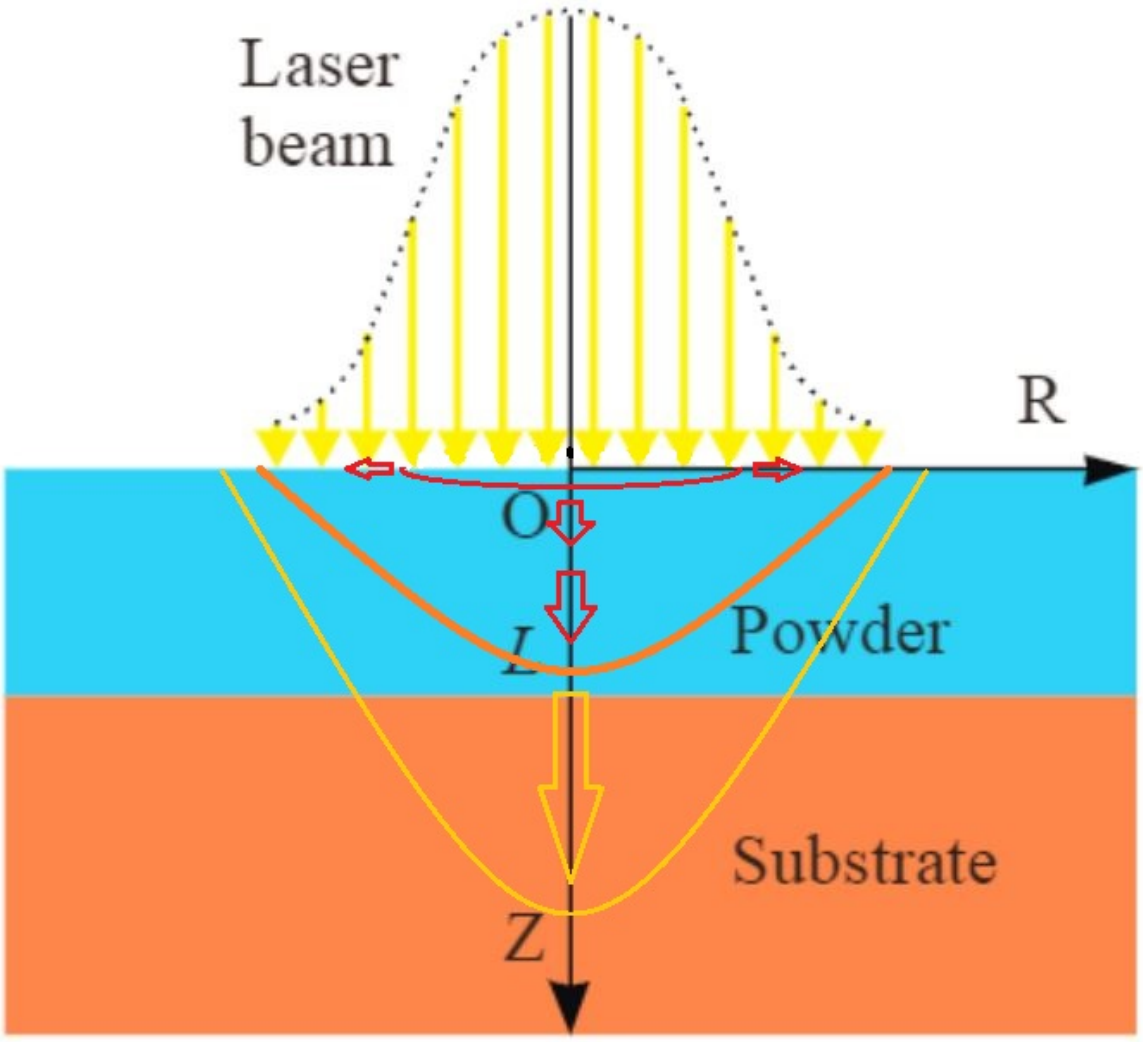

Figure 3. Laser energy is deposited predominantly in the center of the laser spot and then proceeds outward and downward by thermal transport. This is a 2D cross section of the circular laser spot. Once connection has been made with the buildplate, the conduction in that direction dominates and cools the part [13].

At the center of the laser beam, the power deposition is high enough that the metal is vaporized and a plasma forms on the surface. This results in the ejection of particles and agglomerates seen as sparks leaving the print area [14]. However, this can be minimized by tuning the laser power in combination with the laser scan speed to ensure that sufficient energy to melt the metal powder is deposited without

dramatic overheating [15]. The minimal energy balance allows for capillary stability of the melt line preventing balling and lack of fusion defects [12, 13]. A graph showing the ideal balance of speed and power is shown in Figure 4.

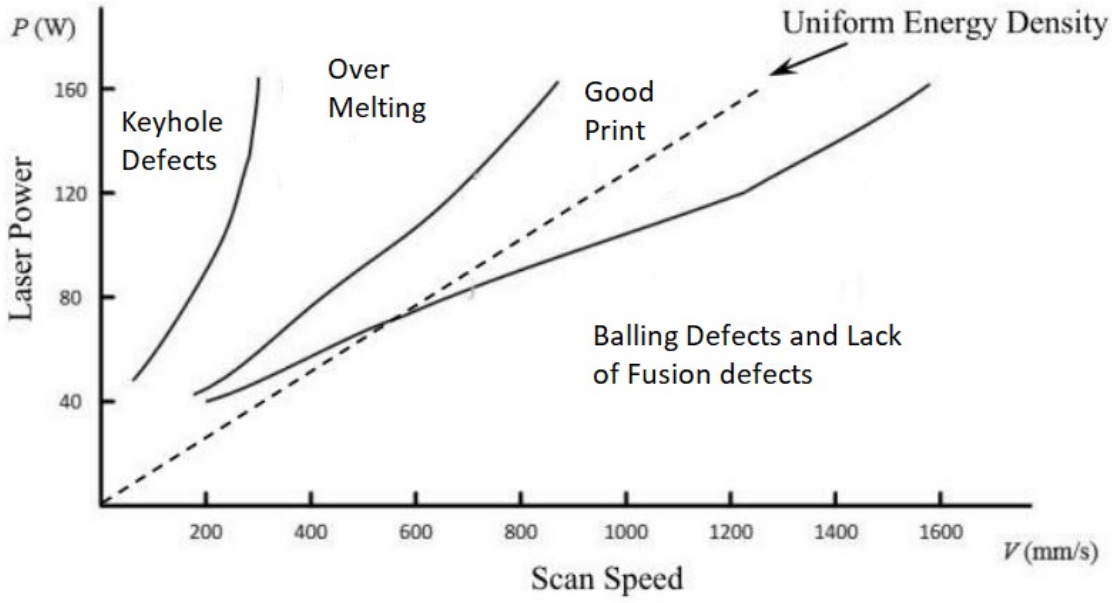

Figure 4. Velocity vs. Power showing the optimal printing balance. The regions represent various density effects. This curve does not come from Inconel 718. However, despite differing alloys, the graph consists of the same general regions [1].

Balling defects can be seen in Figure 5. The maximum energy deposition is dictated by excessive vaporization of the powder forming keyhole defects.

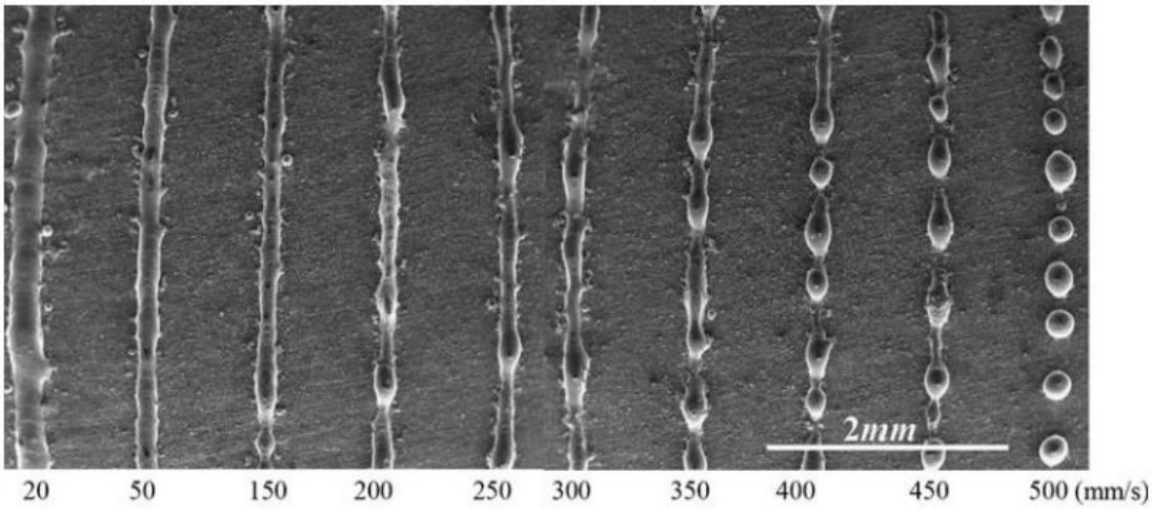

Figure 5. Balling defects as shown above result from rapid laser movement that does not allow for capillary stability of the melt track [1].

Following the irradiation of the core melt area, the surrounding powder comes into play. The most significant heat transfer mechanism for the melted pool is through conduction [8, 9, 13, 16]. Conduction into the surrounding powder is governed by the conduction rate through the fluid, air or melted metal, that fills the gaps between powder particles and initially the conduction is equal in all directions as long as there is powder in all directions [12, 13]. In addition to the growth in the melt pool through this mechanism, as laser power continues to couple in the expansion of the metal vapor that forms in the melt pool also consolidates particles from the surrounding region into the melt pool. This causes denudation, the removal of powder in the area immediately surrounding the melt pool [14]. A general diagram of the powder and melt pool surrounding the laser spot is shown in Figure 6.

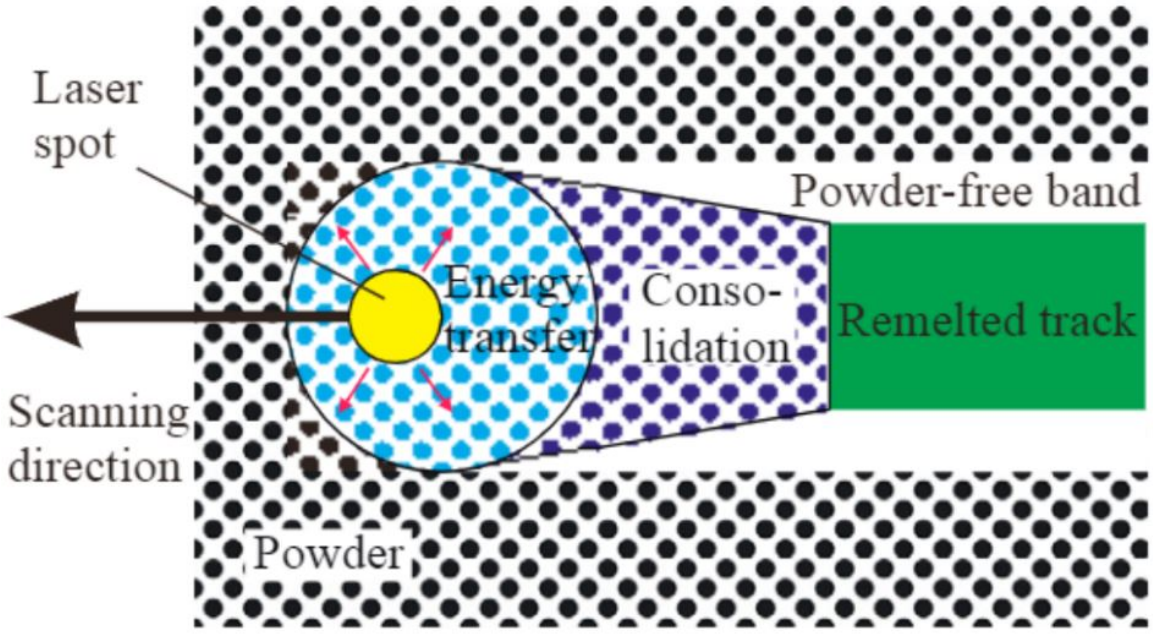

Figure 6. As the laser proceeds the melt track consolidates and brings powder from the neighboring areas into the melt pool exposing the underlying material. This is called denudation and leads to some noise in the cooling data [13].

The omnidirectional conduction continues only until a preferable conduction pathway is formed. This occurs in most components when the powder has been melted down to the previous solid layer. At this point conduction in the negative Z direction dominates. The contact width to the solid layers dictates much of the cooling behavior. The conductivity of the melt approaches that of the solid metal as solidification proceeds [12].

The solid material cools to ambient temperature through the lower print layers into the build plate. When sufficiently far from the build plate, this conduction can be treated as into an infinite bar in the z direction [9]. These heat transfer mechanisms significantly impact the temperature profile and cool down rate of each part of the printed layer as it progresses from powder to a liquid state then into a solid part.

2.3 Defect Formation and Detection

The mechanisms for the formation of void type defects such as keyholing and lack of fusion defects are somewhat understood and help to clarify the impact of the print parameters on the part quality. LPBF is known primarily for the formation of these two defect types. These both result in pores within the constructed material, but the structure of these pores and their formation mechanics are divergent. For keyholing defects, small voids are formed by the trapping of many small pockets of vaporized material shown in Figure 7.

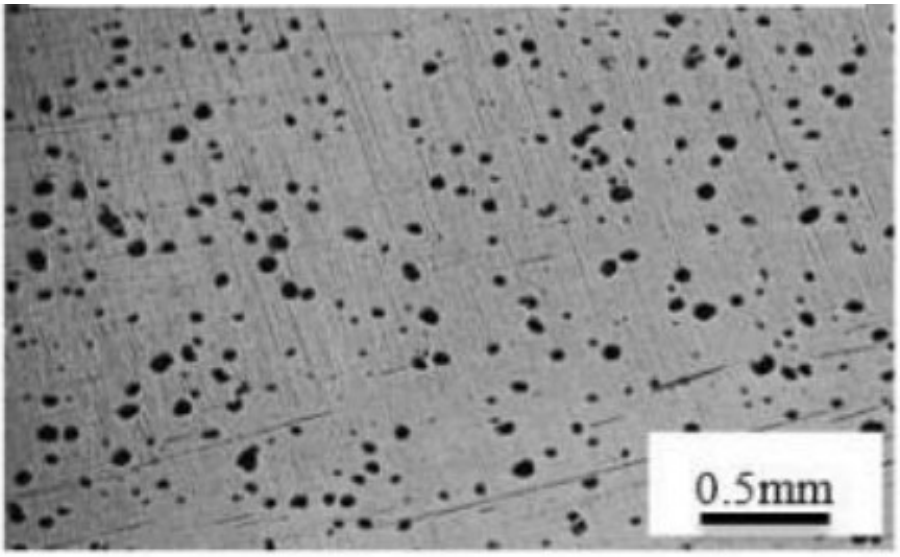

Figure 7. Keyhole defects are caused by overheating. Small pockets of vapor are trapped in the melt and solidified into voids. This is typically caused by a combination of low scanning speed and high laser energy [1].

This is supported by the correlation of keyhole defects with overheated and low conductivity areas. The pockets in keyhole defects can be much smaller than other void forming mechanisms and for this reason they can be the most difficult to detect.

Another form of void is lack of fusion (LOF) defects. These are formed as the result of poor adhesion between the layers of print or print tracks. This is caused

primarily by not enough energy being imparted on the powder. This results in either a separation of the layers by unfused powder or a weak seam between the layers. Either way, the residual stress of the solidification is sufficient to break this region and cause a separation forming a void in the otherwise solid part. These voids tend to be larger than the keyhole defects, but can still be too small for the naked eye.

Over-melting, thermal-stress deformation, and other non-void defects are found in LPBF-AM components. However, the Keyholing and LOF defects represent two of the most difficult to detect via existing means.

The detection and prevention of keyholing and lack of fusion defects has formed the basis of a large area of study in recent years. Some researchers have studied of the impact of observable, user-defined, parameters on the formation of these defects. Others have focused on derived parameters, those which must be observed using additional equipment. They found the defects are caused by the combination of the laser beam power and scan speed [17]. Some of their results are shown below in Figure 4. It shows regions where the balance of scan speed and laser power results in different microstructures and defects. This chart can be made for any of the metal alloys though experimentation and modeling. This method of looking at user-defined parameters and their impact on part quality is referred to as observable parameters due to their inherent availability without any extra equipment [10].

The other approach is to observe some signature of the print using external equipment and correlate it to the part fidelity. This is called derived parameters due to the necessity of additional equipment and the correlation of the observed parameter to the part fidelity. This is an area of research interest as there are many potential parameters which could be related to the part fidelity.

First, derived parameters can be observed during the print (in-situ) or after the completion of the print (ex-situ). Some observation techniques cannot be integrated

into the print process easily, including CT. Others, including sectioning and inspecting via Scanning Electron Microscopy (SEM), require that the part be destroyed after completion. These ex-situ processes have benefit mostly in being well established techniques used for AM and other manufacturing. The process of inspection is simpler, albeit less effective than trying to observe the print in process. However, these processes have significant limitations. The first is that they are inherently wasteful. If a part is found to be defective, it is unlikely that it can be fixed and so the whole part becomes scrap. Beyond that, the destructive techniques guarantee that the part which is inspected is destroyed and in order for statistical methods to be of any use, a substantial sample size is required to determine the norm of a part before even one part can be produced with confidence. This is inherently counter to the customizability of AM. Destructive testing is not compatible with the AM paradigm. It is unlikely that the ex-situ processing will present a scaleable efficient quality control measure and so in-situ processes have dominated the edge of research.

2.4 In-Situ Diagnostics

Because of the many ways the build can be observed, in-situ diagnostic methods are themselves a very diverse field. There are a few divisions which can illuminate the approaches taken in recent history. Most rely on imagery of the build layers. Infrared (IR) imagery, visible imagery, and interferrometric imagery are the main three categories. Within each method, they can image effectively one, two, or three dimensions.

IR imagery is commonly used for determining radiometric temperature maps because objects at typical temperatures emit in the IR. IR signatures have been correlated to temperature of the pixel. This is possible due to the functional relationship between temperature and hot body emission defined by 1.

$$M = \int_{\lambda 1}^{\lambda 2} \epsilon(T, \lambda) BB(T, \lambda) d\lambda \tag{1}$$

This relationship is fairly simplistic except that the emissivity, which scales the exitance based on the material properties, is not truly a constant. It is dependent upon the material and its temperature which leads to a great deal of uncertainty in the measure of exact temperature. Rather than calculating exact temperature, the raw signal from the IR camera is used as an analogue for temperature and many sensing methods have used and proved the effectiveness of using IR imagery as a way to view relative temperature [18]. Whether using IR imagery in its raw form or calibrating said imagery to temperature, both methods are effective at observing thermal properties and thermal evolution of the part through the printing process.

Another option is to view the part with a visible camera. This allows visible changes such as surface roughness, melt pool geometry and debris emission to be tracked. Some properties like roughness are more easily observed visually rather than thermally. These properties serve as some examples of physical properties that can be related to part fidelity, but there are many more. Because of the simplicity of visual image capture, perhaps the least complex approach is to look for the defects with visual imagery as each layer is created [19].

The least common imaging method is the use of interferometric imaging to determine the exact height of each point in the melt pool as the print is being performed [20]. The interferometric topographical image of the surface is formed by reflecting one half of a split beam off of the surface and comparing the offset of the wave to the other half that has a constant path. This method produces very sensitive topographical information of the melt pool and solidified surface that can indicate the print condition. This method is especially interesting due to its high degree of sensitivity,

but it is very limited in the types of errors which it can detect. All defects must create or correlate to a significant change in the melt pool or the surface roughness.

Information of varying dimensionality can also be collected. Since measurements in one and two dimensions can be combined into higher dimensions, this is not as distinct as imagery type. The first is one dimensional or point analysis. Typically this is performed by looking only in the immediate vicinity of the melt pool. This is most easily achieved through coaxial imaging by using the same optics being used to steer the laser around the print as these optics operate in the same path forward and backwards keeping the collection method directly aligned with the laser spot as shown in Figure 8.

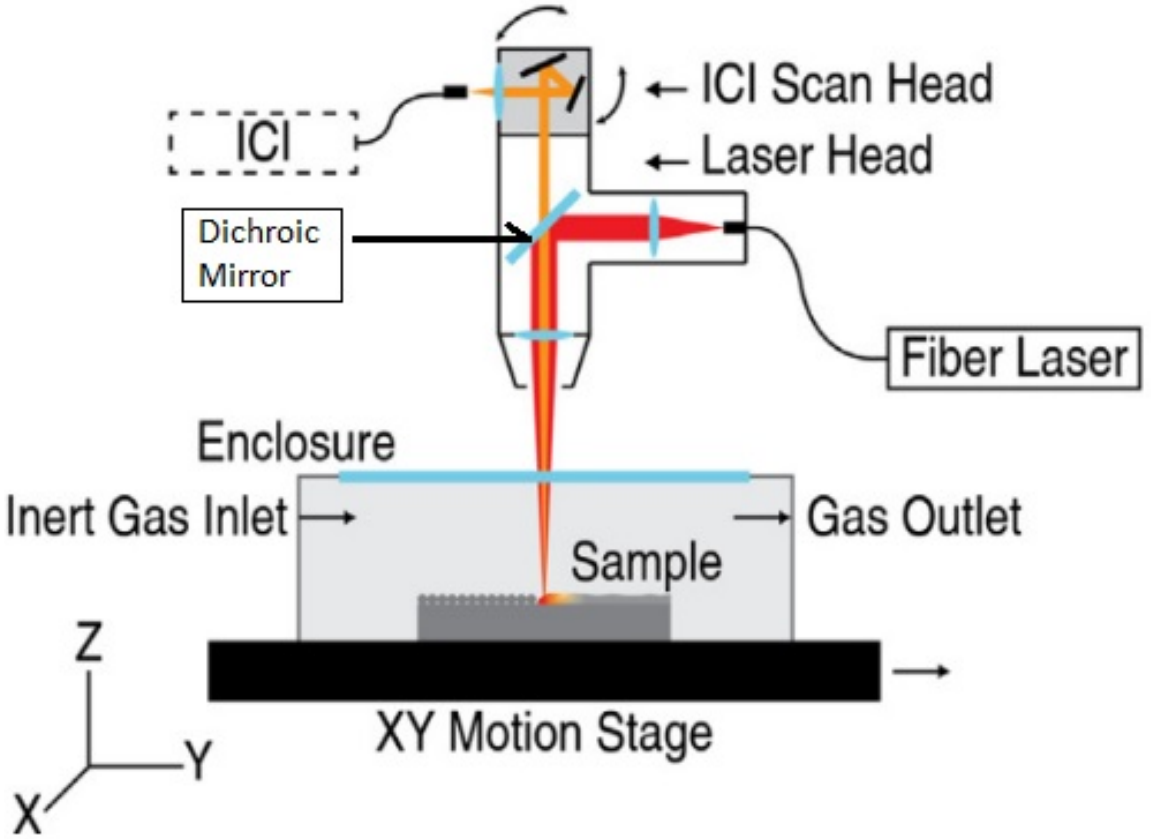

Figure 8. Coaxial imaging schematic shows the shared optics and specifically a dichroic mirror that redirects the wavelength of interest to the imaging system while avoiding the laser wavelength [20].

This imaging comes with the challenge of avoiding the exact wavelength of the laser and ensuring that the optics are designed in such a way to accurately steer the observation wavelengths in addition to the laser. This is particularly difficult if the wavelengths are significantly different or if the optics are wavelength dependent. In order to avoid this, some techniques instead choose to steer the collection system with separate optics and follow the laser point. They observe many of the same properties like melt pool temperature and shape as the co-axial setup, but encounter different limitations and challenges. Neither method can effectively track changes over time, but many observations like peak temperature can be made about the print at the

moment of heating. Peak temperature has been correlated to defect production. This method also allows for the gathering of the least amount of data that can still provide useful indication of part quality [8, 16, 21, 22, 23, 24].

Imaging in two dimensions is the most common method used due to its simplicity, because the observation system is set up to observe the entire area of interest and passively collects data for the entire area during the print. However, this method produces a great deal of extra data of areas that are not bring printed which can prove to be a challenge in data processing. However, this method allows for the monitoring of the entire area of the build over time which can find the changes that the single dimensional snap shot approach cannot find [9]. It is also capable of observing all of the same parameters as the single dimensional approach [25]. This allows for the combination of a number of different parameters like the cooling behaviour and peak temperature as well as the comparison of these parameters in equal conditions. Additionally, the two dimensional methods can be simplified to single dimensions by discarding all data except the region around the laser spot or combined into three by stacking the observed layers.

The three dimensional approach is only achievable as an in-situ analysis by combining the two dimensional images into larger structures in order to track changes over the entirety of the build. This is especially helpful in trying to compare the behavior of the part to computational models of what the thermal behavior should be based upon the structure [26]. This approach is limited predominantly by its complexity. It is computationally intensive and although the measurement is taken in-situ, it is combined with the thermal model in post processing by necessity and cannot be performed easily during the build. The dimensionality of the approach can limit what can be observed and the amount of data captured on each later via this

the sensing method; however, restricting the dimensionality dramatically reduces the data overhead required to capture, transfer, and store the measurements.

2.5 Process Monitoring

Many approaches have attempted to answer the challenges of process monitoring discussed in Section 1.3 but typically it becomes an issue of sacrificing one parameter for the sake of another. One such approach is to attempt to get the most detailed and noiseless information possible about the quality of the print and disregard the issues of data quantity and calibration. It is possible to create an accurate computer model and predict how a particular processing parameter such as temperature should appear and evolve then compare this to the actual findings [9]. Even more complex than this is to create a complete model of the component representing the part to actively compare with the measurements of temperature [26]. These methods are generally very computationally expensive. Additionally, they require a great deal of information and effort before the print and the flexibility of this approach is limited. These methods tend to use IR imagery to find exact temperature. They are founded deep in theory and account for almost all of the noise and variation in the parts. This allows for very accurate detection of defects, but using a lot of processing power, making these methods most useful for ex-situ monitoring.

Another approach attempts to handle noise without implementing complex simulation or modeling, but by using machine learning algorithms to separate the noise from the data. This is conceptually interesting because the patterns of thermal or physical properties are often visible to a human eye, but the computer struggles to find the same pattern by simple statistical rejection. One of the machine learning algorithms can separate some of the regiospecificity from the data as there is a good deal of consistent variation across the viewing area [25, 27]. This helps the patterns

to become more visible and machine learning is effective at detecting the patterns and separating them from the background. Additionally, given enough training data, machine learning can be used to effectively form a predictive characteristic of a particular spatial parameter such as the melt pool geometry and effectively predict when that parameter exceeds the acceptable bounds [22]. These methods, although highly accurate, do not facilitate the active monitoring of the print on their own because of the challenges in computation time and even exacerbate the challenges of data capture and transfer.

The opposite approach has been to take the simplest measures available like peak temperature, potentially reducing the data capture and processing expense, and investigate their applicability and sensitivity. If more complex systems can be used to indicate the presence of a defect, can some related, simpler system detect the same defect to a sufficient degree? This is the approach for systems that look at the peak temperature, assuming that the lack of conduction can lead to overheating in the material [18]. This method showed some promise being able to detect relatively large defects. Another approach has been to connect some of these relatively simple parameters with the observable parameters mentioned in Section 2.3 such as the scan speed and laser power [10]. These methods tend to be able to give an indication of how likely it is that an error occurred, but not whether an error actually occurred or where it may be located. This statistical approach is acceptable for some applications, but not for high demand applications.

2.6 Seminal Research

A series of studies has investigated conductivity effects in fine structures. It was found that the conduction through underlying powder is nearly equal to open air and both are dramatically different than conduction through solid metal [8, 9, 16, 23].

Additionally, the conduction is affected to a lesser degree by the thickness of the fine structure beneath the surface [26]. This suggests that the conduction away from the surface is a highly sensitive indicator of the bonding to the underlying layers, an indication of part quality beneath the surface. Since fine structures are of particular interest in the AM field, being able to accurately predict defects in such products be of great benefit. However, in order to accurately detect differences in conduction as simply as possible, a good analogue for temperature is required.

As discussed in Section 2.4, IR emissions can be calculated to temperature with proper calibration and knowledge of surface emissivity. This implies that IR emission intensity is correlated with temperature and could be used to detect relative differences in sub-surface conductivity. Previously, the maximum IR intensity has been used as an analogue for relative maximum temperature with success [8, 18]. By using this maximum temperature idea, previous studies have been able to show that areas with more direct conduction pathways do not reach as high of maximum temperatures shown in Figure 9. Despite this promising indication, this method lacked precision and sensitivity. The Figure 9 was predominantly open structure with increasing numbers of conduction pathways.

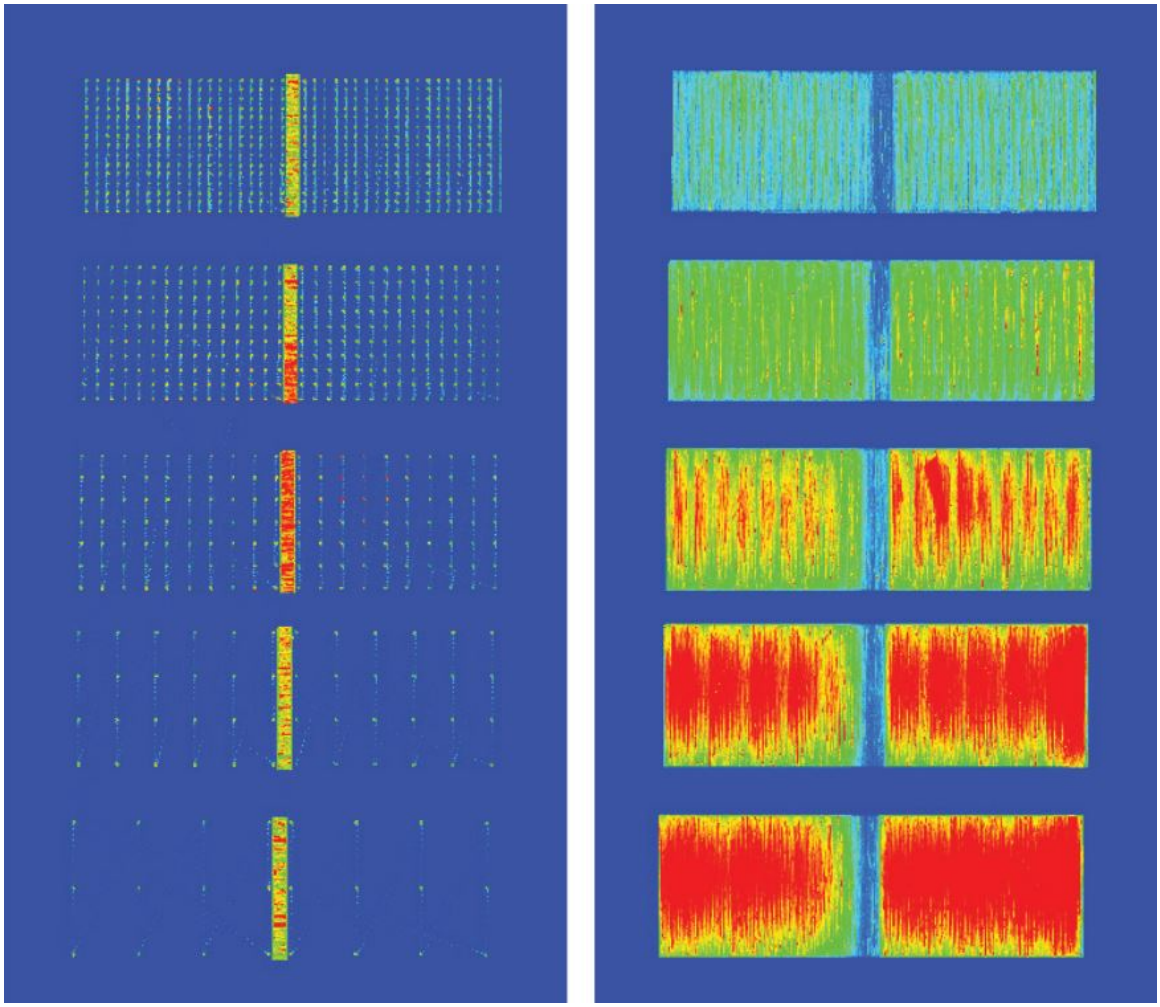

Figure 9. The maximum temperature was shown for a series of open geometries with increasing numbers of conduction pathways. The sensitivity of this method was not designed to be able to detect small sub-surface defects, but it successfully found over-melting for overhanging structures [23].

It has been stated that the conductivity is an appropriate parameter for predicting the part quality through intensive computational modeling [9]. This method was much more sensitive to defects than maximum temperature shown in Figure 10, but was computationally prohibitive. The goal for removing temperature calibration as well as complex modeling is to bring the computational expense within a reasonable limit. These discoveries have led to the belief that a sensitive, simple parameter can be

detected in the form of a analogue to conductivity from the decay of the IR intensity at each point in the build over time.

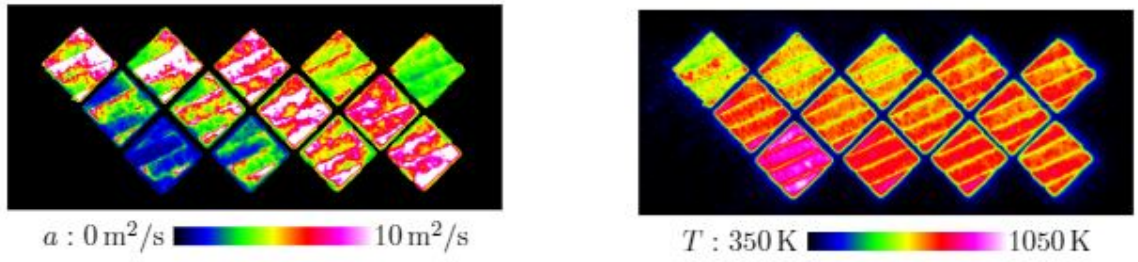

Figure 10. The conductivity term painstakingly calculated (Left) shows an indication of the subsurface defects (located in the left cubes). Where the maximum temperature (Right) only indicates one cube as having anomalous cooling behavior (the leftmost bottom cube) [9].

To achieve a balance between these two methods raw measured IR signals were used to create a relative cooling curve for each location in the build by plotting the change in IR intensity over time. This plot is fit to a model analogous to the equations for temperature evolution over time as a result of the typical means of thermal transport and then the conductive component is extracted and used as an analogue to the conductivity of the material at that point.

III. Methodology

The goal of this research was to gather infrared imagery of each print layer throughout the print and correlate that data to print quality. Defect layers were included in the print file by design to have a clear indication when a parameter was effective. Previous work indicated that estimated the conductivity by monitoring the cool-down behavior of the surface would be possible. The data was processed with the goal of creating a parameter map indicating part quality.

3.1 Printer Set-up

Figure 11. ConceptLaser Cusing M2 3D Printer used to produce test components.

The printer used is a ConceptLaser type M2 cusing shown in Figure 11. The printer is equipped with a single mode, CW Ytterbium fiber laser, operating at 1070 nm with a minimum beam diameter of 50 μm, power of 120 watts, and 280 mm/s scan speed. The print was conducted under an inert 99.9% Argon atmosphere to prevent the rapid, explosive oxidation of the metal powder. The metal alloy powder used in all test prints was 10-20 mum particles of Inconel 718. This nickel superalloy is used in many aerospace applications and is a superior welding alloy, highly conducive to 3D printing. A single pass of the laser in a circle was used to achieve the smallest thin wall structure possible and to increase the sensitivity to skipping single layers. It also allowed for the observation of the entire cooling behavior to the noise floor without the reheating due to adjacent laser passes.

3.2 IR Camera Set-up

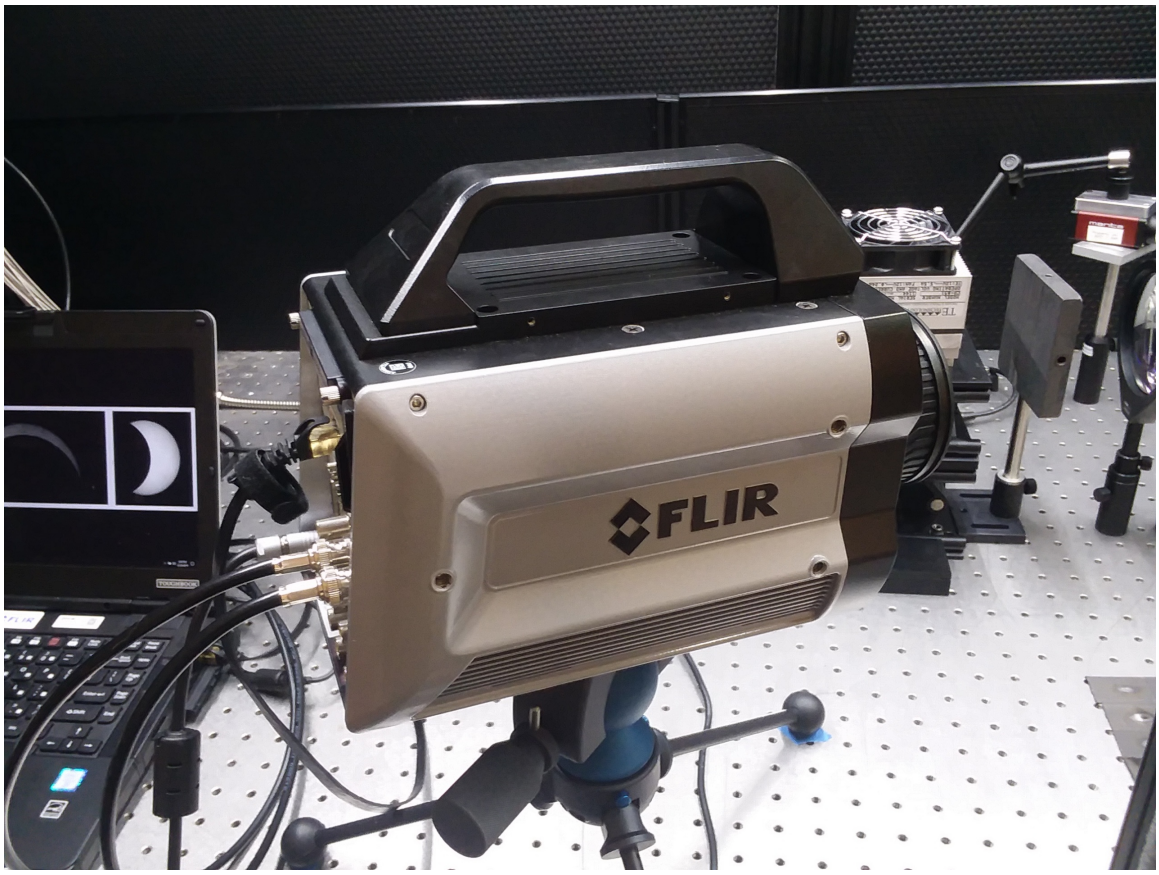

Figure 12. FLIR SX-6901 Camera used to image test components.

The camera used to collect data was a FLIR SX-6901 mid-wave high-speed imager with a 512x640 InSb array shown in Figure 12. The data was captured as .sfmov files with a frame rate of 1000 Hz and an integration time of 10 μs, providing excellent time resolution of the melt peak and enough dynamic range to view the initial peak through the region of interest. The camera was not integrated into the printer operation, but was triggered to start collecting imagery manually for our data collection. The camera was triggered at the end of the powder spreading step and captured the entire laser path and some trailing data due to the fixed capture time of ten seconds. The integration time was set such that the peak of the melt pool was not totally saturated.

A single integration time, ten microseconds, was used to capture the data in the region of interest, consisting of two or three rings covering less than ten percent of the build plate. The camera was mounted inside the outer housing of the printer but outside the build chamber looking through an IR transparent Germanium window using a custom built replacement for the back wall of the printer as seen in Figure 13a. There was a 3.8-4 μm filter used to restrict the wavelength and intensity of light so that future work could be performed if accurate temp correlation was desired.

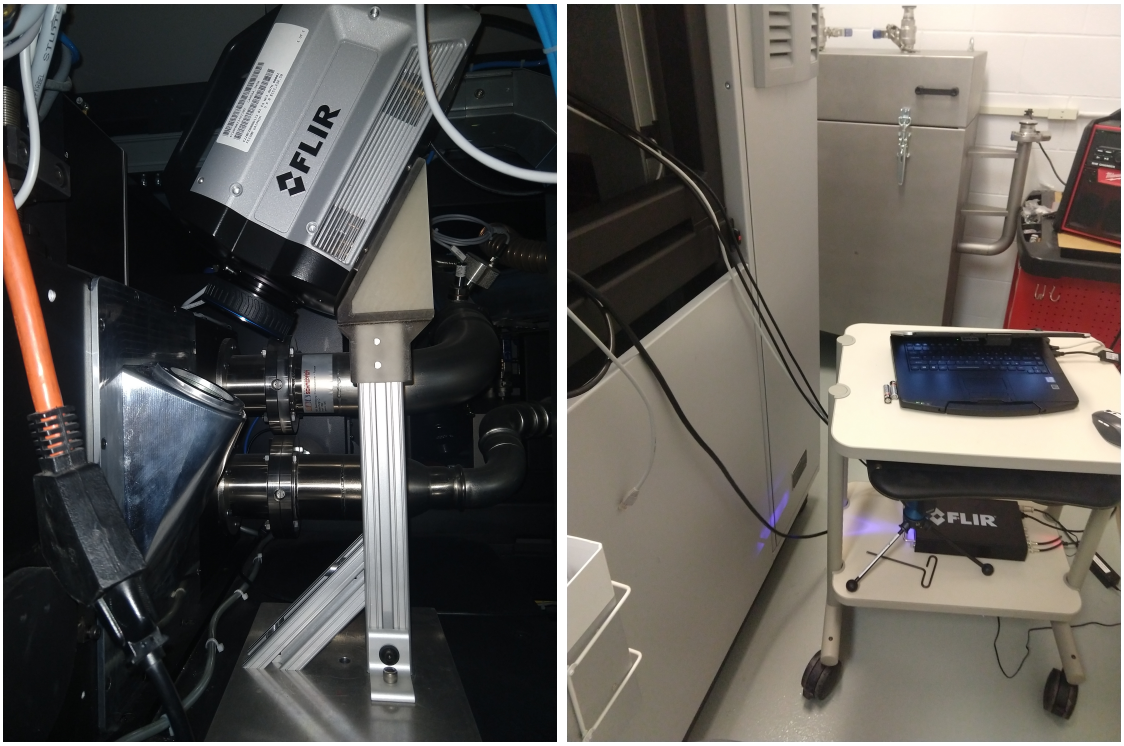

(a) Mounting System. (b) Control Station.

Figure 13. The mount used inside of the LPBF-AM printer and computer used for controlling the camera.

The camera was mounted on a separate stand, held in place over the view port with some space to set the distance to the plate in the middle of the available focal lengths. The camera was fixed at an angle and could only focus on the region of

interest consisting of less than ten percent of the plate. However, this was not a limitation of our data collection since it did cover the necessary portions.

The camera was connected to an external control computer and an integrated High Speed Data Recorder (HSDR). The connections were routed within the printer through a side access panel and the control station located next to the printer as shown in Figure 13b.

The camera was controlled within FLIR's ResearchIR software using the record function connected to the HSDR. The capture was set to record for ten seconds due to the lasing lasting approximately five seconds and the full layer deposition and print lasting fifteen seconds. Manual recording was inefficient and about twenty five percent of data that was not captured fully due to human error. For this reason, a triggering mechanism that consisting of a switch actuated by the powder spreading arm and sending a signal through the camera's auxiliary was investigated with the help of FLIR technical support, but was not able to be implemented in the time available. This would reduce the human error in triggering the system at the proper time and would improve data collection consistency. During the print, the data is quickly transferred from the camera to the HSDR via a high speed coaxial cable. Following the print, the data is then transferred to the computer from the camera via a slower Ethernet cable. The data can then be transferred onto an external hard drive for transport or processed on the machine.

3.3 Print Design

The print was designed as two thin walled, about 180 μm ,rings twenty-five millimeters in diameter. In order to induce a detectable defect, the print was designed with portions of the thin walls skipped for multiple layers before resuming continuous layers as normal. The intention was to induce a powder separation in those regions

that would show a detectable difference in cool down behavior. The four quarters of the ring had slightly different build instructions. The first hundred layers were built as solid rings in an effort to move the target area away from the build plate and induce consistent conduction.

Following the pre-defect layers, the defect print pattern began. The pattern consisted of a section of skipped layers followed by solid layers making up twenty-five total layers per defect cycle. The four quadrants of each ring were printed with different numbers of skipped layers. One ring was printed with zero, one, two and three skipped layers. The other ring was printed with zero, two, four and six skipped layers. The design is shown in Figure 14.

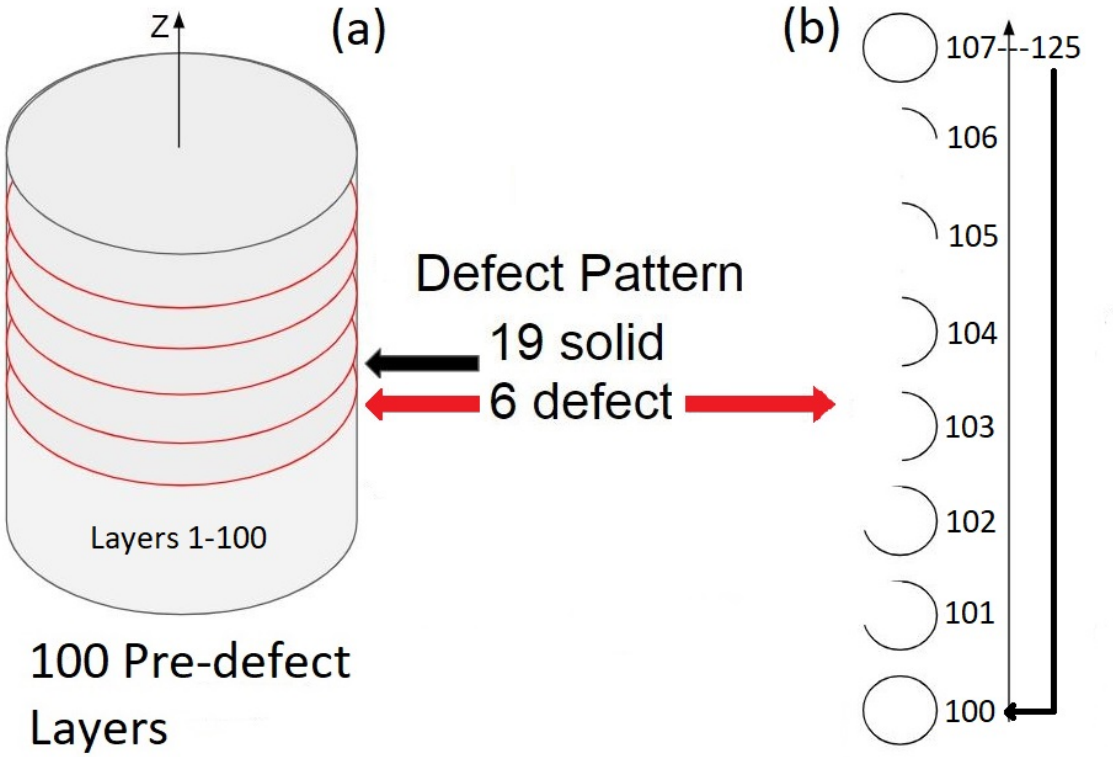

Figure 14. The entire print design for the first print (a) is shown with the hundred pre-defect layers and the defect design of 6 defect layers (shown in red) followed by 19 solid layers for each defect cycle (b) the pattern for the double skip tube.

3.4 Data Processing

The large imagery data files were transferred to a larger computer with more RAM for processing. The data was read into MATLAB R2017b where the raw .sfmov files were converted into MATLAB matrices. At this point, videos were produced from the matrices that still had accurate temporal data to visually confirm some critical areas of the print and ensure that the print matched the prescribed design. The code to convert the files to .mat also compressed them by setting to zero all of the matrix values determined to be at or below the noise floor and eliminating all zeroed values then collapsing the matrix. The noise floor was set to cut off data just above the average of the bottom twenty percent of pixel values, at just below one-thousand counts. This was determined to be appropriate because there was only a small percentage of pixels which captured higher temperature pixels. This removed the temporal relationship between neighboring pixels, but maintained the temporal order of the frames above the noise floor for each pixel independently. This produced 3D (spatial, spatial, temporal) data cubes that were then processed at each spatial pixel as two dimensional plots of time (t) versus the IR camera output intensity (I) in counts. These plots were then fit to a model for the cooling rate which was based upon the three heat transfer mechanisms (conduction 1st term, radiation 2nd term, convection 3rd term). The model is shown in Equation 2.

$$I = A * e^{-k*t} + C * t^{-D} + E \tag{2}$$

This model was fit to the data at each pixel via a least squares fit regression using the lsqcurvefit MATLAB function. This function produces the regression information including the mean squared error and Jacobian matrix, as well as the final values for the constants in the functional model. As will be shown later, the conduction and

cool-down rate is an indicator of part fidelity and so the k value (designed to be an analog for conductivity) was analysed to determine if there was a pattern in the data which matched the designed defect pattern from Section 3.3.

To reduce the noise, one step was to plot the Z scores of the k-values. Z scores are a measure of the deviation of the value from the mean. This is often used to determine if points are substantially different from the general population of data like outliers. This was calculated by 3.

$$Z = \frac{X - \mu}{\sigma} \tag{3}$$

This value indicates the separation from the mean in terms of the standard deviation and reduced the range of values so that they could be more easily visualised with a single color bar. Additionally, the Z score helps to quantitatively determine which points belong in the data and which are noise. The separation and noise identification makes any pattern more apparent with the help of Z scores.

IV. Results and Discussion

Clear four quadrant gradation matching the designed defects was observed through the cool-down rates from the IR imagery. This indicates that the model fit parameters which we observed accurately detect changes in the conductivity of the material. This was found in both prints. Two prints were performed with the same parameters and different designs. The first print consisted of two tubes printed and the second was three tubes. Code was completed to analyze both prints following the first print. A number of difficulties were encountered, including errors in the printing process and challenges in reducing noise, which initially obscured the defects. However, through data processing and noise reduction, the defects emerged from the data.

4.1 Separation from the Build-Plate

In order to get more consistent conduction described in the last chapter, solid layers were printed before the defect pattern. The leveling off of the conduction was verified by plotting the conduction as a function of layer height for the pre-defect layers and a consistent trend was found shown in Figure 15.

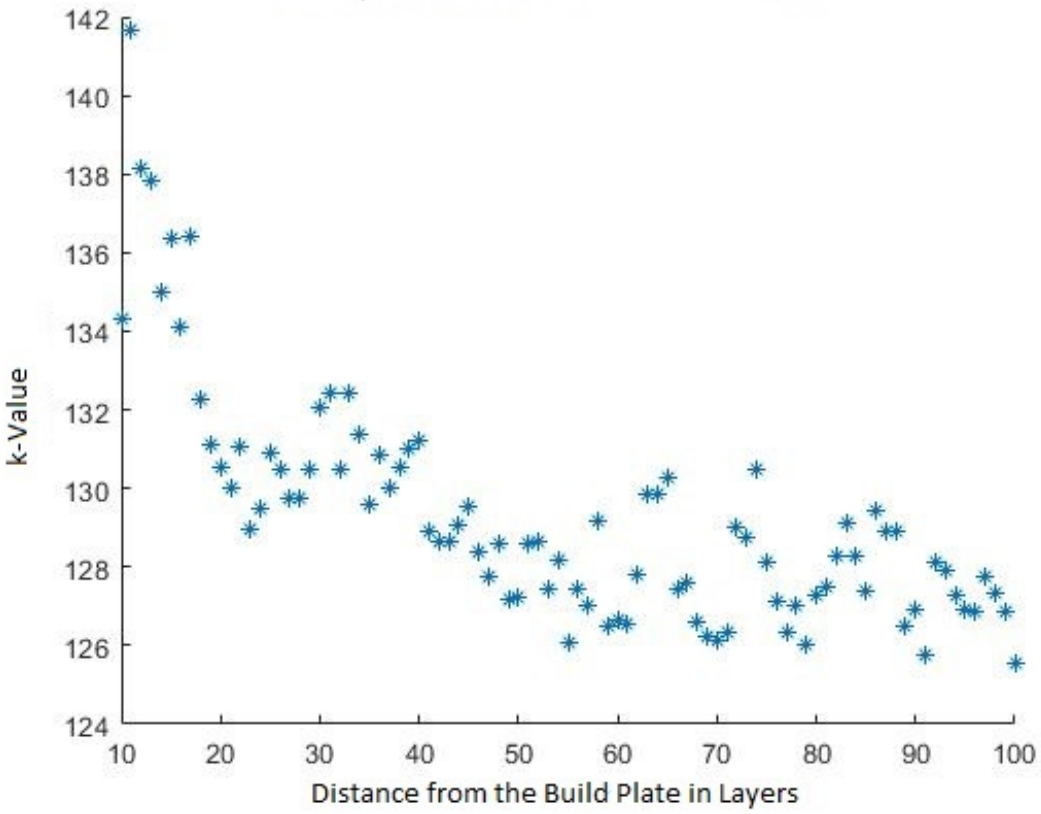

Figure 15. The distance from the build plate had a consistent effect which leveled off prior to the defect pattern.

Figure 15 empirically supports the common practice of building extra layers before printing the intended design. The consistency of the conduction after these extra layers makes the finished part more homogeneous. This helps avoid defect formation. Additionally, the detection of the expected change in conduction through the k-value further validates the use of this variable as an analogue for conduction.

4.2 Errors in Printing and Data Collection

The goal for the print was to skip enough layers to induce a region of unmelted powder that would remain as a void in the part after a solid layer was printed on top

of it. However, the design used for the first print did not achieve the desired result in the part. The amount of over-melting was severely underestimated. The unmelted powder completely fused by the solid printed layers above the defect resulting only in a variation in thickness at the location of the defect, rather than a void. This is shown in Figure 16.

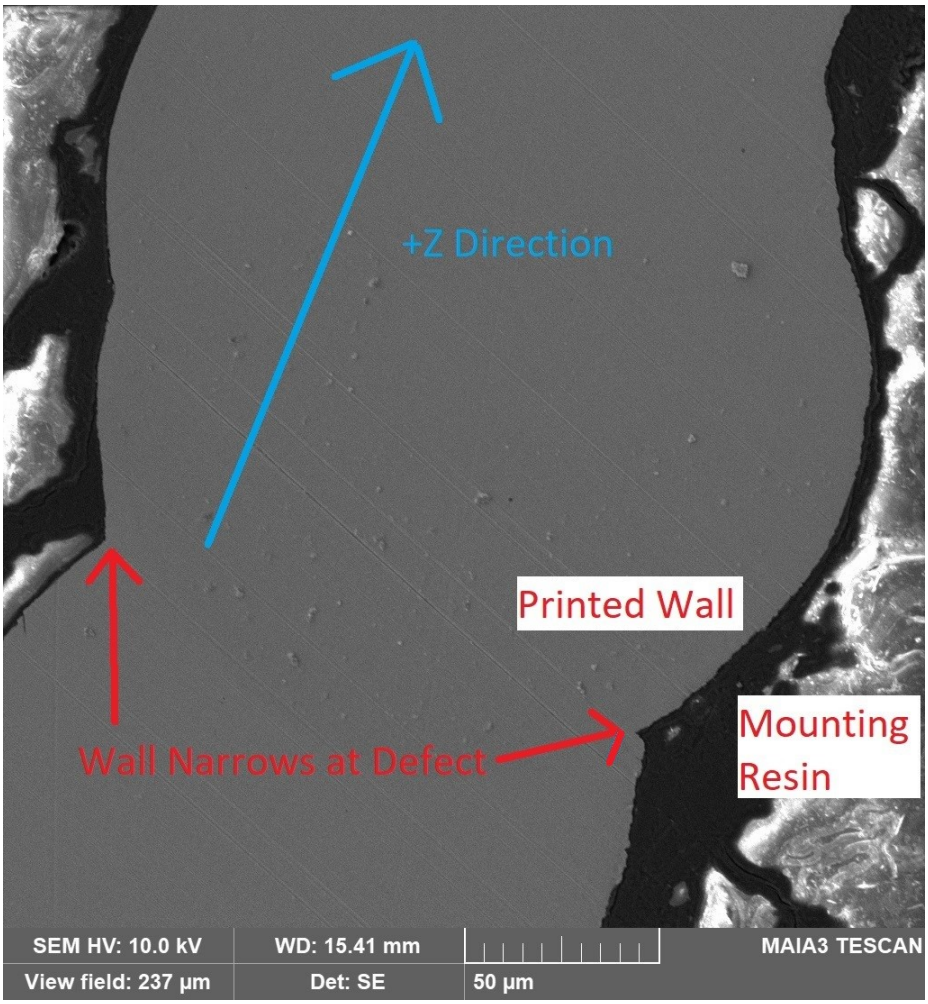

Figure 16. Shape of the resultant defect produced by the over-melting and resealing of the unmelted powder.

The reduction in thickness beneath the surface does reduce the conduction [26]. However, the reduction is much less than would be expected if a void had been

produced. Despite the fact that the conduction was not impacted as significantly as designed, the reduction was still sufficient to be detected. This highlighted the sensitivity of the method.

In the first printing, an error occurred that caused a whole ring to be printed instead of the defect that was intended for that layer. The error occurred unpredictably. The intended defect pattern in shown in Figure 17a.

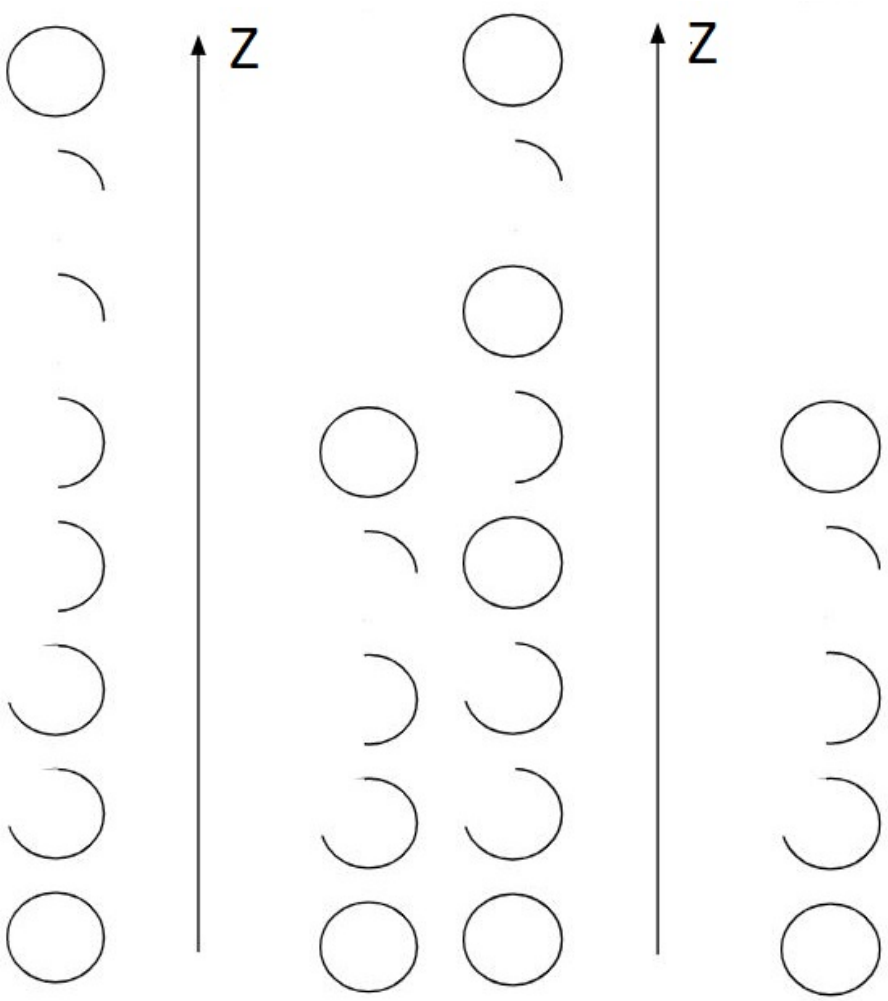

(a) Intended defect pattern. (b) True defect pattern.

Figure 17. Intended versus true defect pattern for the double skip ring.

However, due to this error, the pattern changed between each layer with various

effects on the overall defect structure based on where in the print was skipped. An example of how the defect prints changed is shown in Figure 17b.

There were some locations where the error effectively removed the defect and some where it was relatively inconsequential. Additionally, there were challenges in capturing the data in its entirety. Because the camera was being triggered manually, a number of the layers were triggered too late, without enough time before the print began. This resulted in losing some or all of the layer's data. More data was lost throughout the print likely due to user fatigue, but enough layers were fully or mostly captured to get a clear picture of the trends and all defect patterns were captured within one to three layers before and after the print. The effect of missing the layer immediately following a set of defects is a greatly reduced defect pattern signature. Within two layers, the presence of defects is nearly invisible due to the minor effect that the defects generated had on the conductivity and the resealing of the gap.

For this reason a second print was performed with the goal of skipping enough layers to ensure that there was separation between printed solid parts. This was done by increasing the number of layers skipped to a maximum of forty five layers and was successful in producing separation. However, the separation around most of the ring causes the structural integrity of the part was compromised. This resulted in the sweep arm breaking two of the printed tubes where sections were skipping more than fifteen layers. This made the data in these rings relatively unusable. The most interesting section in this print was the one that skipped five layers at a time. This print was not destroyed by the sweep arm, and the separation produced large differences in conductivity.

4.3 Processing IR Data and Results

The cool-down curves collected from the IR imagery were fit to a simplified heat transfer model equation 2 from Section 3.4. From the Jacobian, each variable in this model was analyzed for independence using a correlation matrix shown in Table 1. Large values for the correlation matrix indicate that the variables corresponding to that cell are dependent upon one another. Values closer to zero indicate that the two variables corresponding to that cell are independent. Additionally, negative terms indicate an inverse correlation while positive indicate direct correlation.

	A	k	C	D	E
A	1	-	-	-	
k	5.70E+00	1	-	-	
C	4.21E-01	9.64E-02	1	-	-
D	-1.65E+03	-2.46E+02	-2.53E+03	1	-
E	-1.35E-01	-4.96E-02	-5.23E-01	1.98E-04	1

Table 1. Correlation Matrix for Variables in Model

The correlation matrix indicates that the D term may be superfluous due to the values in the D cells being multiple orders of magnitude larger, but all other factors are necessary and independent. This suggests that the D term is dependent upon the other terms and could be removed with little effect on the overall model. The term was removed and the reduced model fit acceptably, but not well, as shown in Figure 18. For the reduced model, with the radiative term excluded, the data also became more difficult to analyze due to less relative variation in the k-value. For this reason, analysis was performed on the full model.

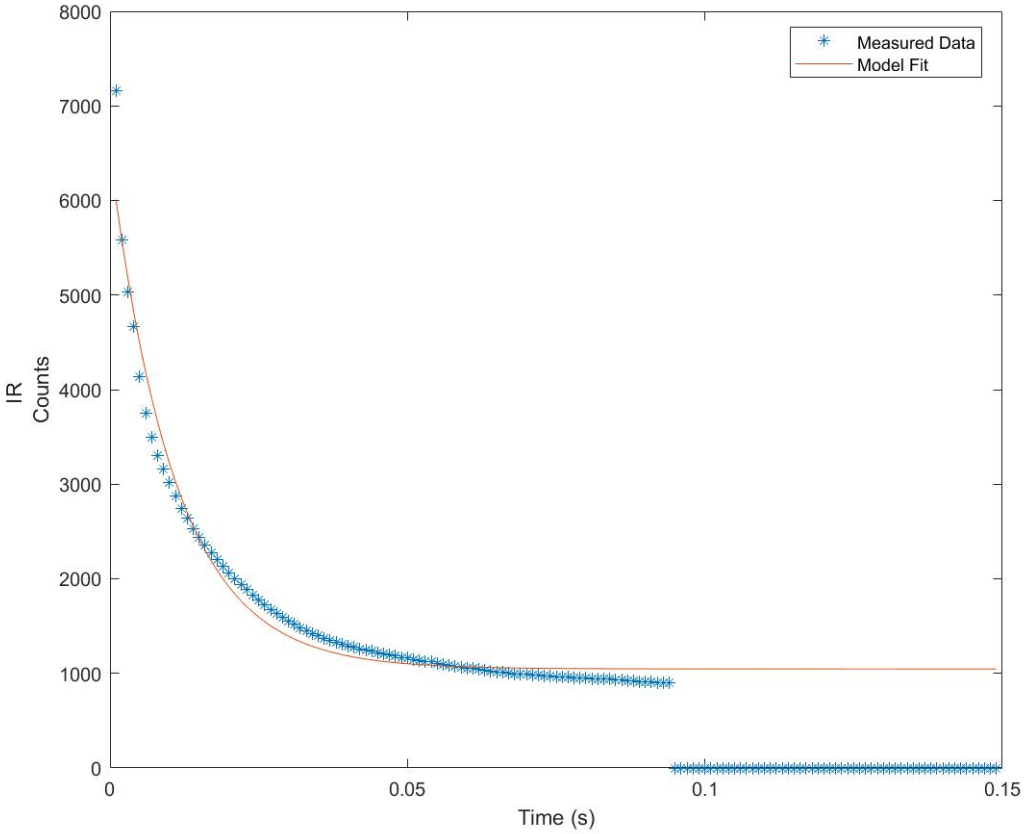

Figure 18. The fit of the model without the radiative term was acceptable, but not as good of a fit as the full model shown below.

This fit to this model was performed for each spatial location in the print containing more than twenty-five intensity measurements above the noise in order to reduce analysis of sparks flying across the screen and other short duration events. The curves fit the non-noise data with low residuals and events such as sparks landing in the powder within frame were fit with highly divergent parameters. An example of these fits can be seen in Figure 19a for a solid region of the print, Figure 19b for the average fit of a large number of data points, Figure 20a for a data point on the edge of the print where the cooling suffers from a denudation effect, and Figure 20b for a spark

that fell within the viewing area. For all of the graphs, the time axis was calculated from the frame rate and is measured in seconds. Additionally, the values below the noise floor (average bottom 20%) were eliminated by the compression algorithm.

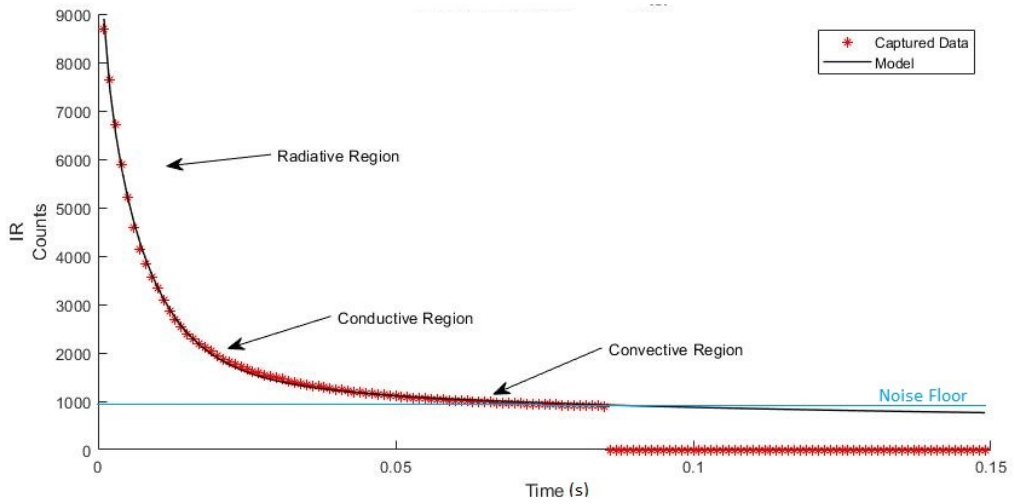

(a) A good print location identified from the center of the wall is plot with its fit curve showing the dominant cooling equation term dictating each portion of the graph.

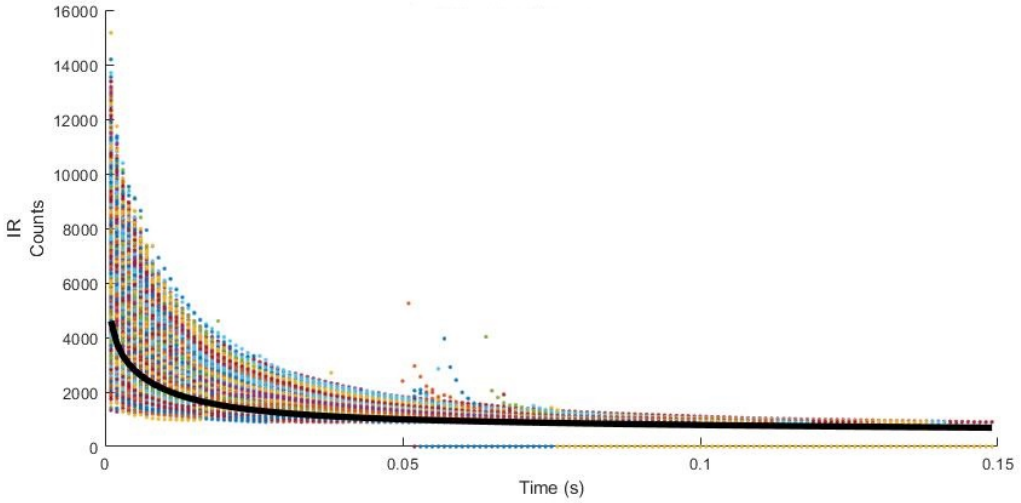

(b) Likely good print locations that passed the noise elimination with a curve defined by their average parameters showing the variety of normal print locations with differing initial values and even some reheating effects.

Figure 19. Overall Model Fit

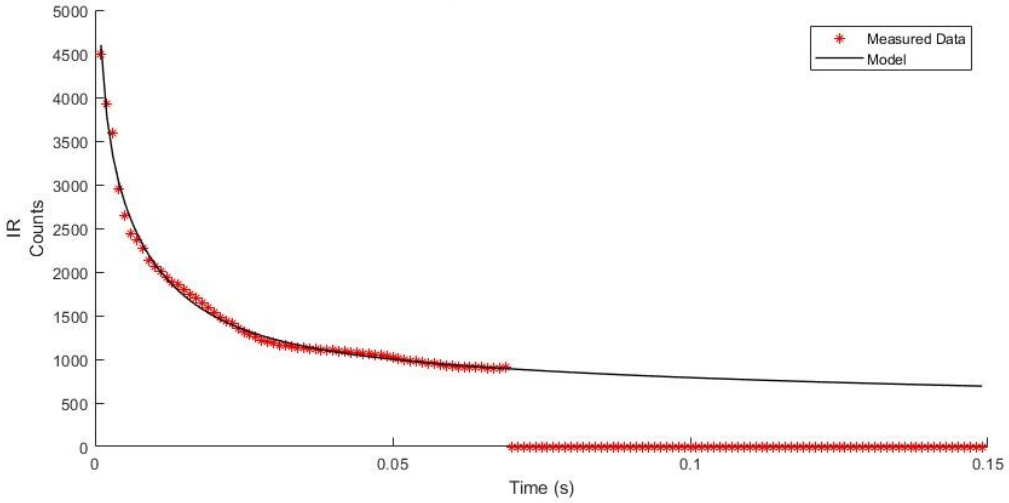

(a) Edge location with its fit curve. The instability and fleeting nature of this data point is likely due to the denudation effect caused by the vaporization of metal and small air currents that result.

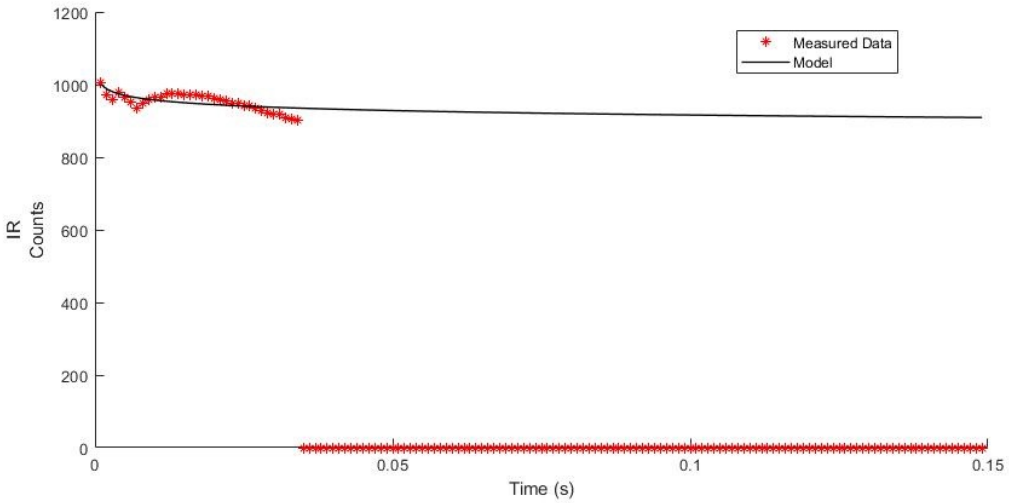

(b) Spark location and its fit curve. The identity of this point was separately confirmed by inspection of the video and its intense but fleeting nature is characteristic of sparks.

Figure 20. Model Fit to Bad Data

All the model fitting parameters were evaluated as potential defect indicator parameters. The k-values of the fits (exponential decay constant) were analyzed in depth due to their expected similarity to conductivity. The first step was to create

an image of the k-values for each layer prior to and following the printing defect. This approach was relatively ineffective because the random variation obscured the difference in k-values for the different defect regions. One of the initial images can be seen in Figure 21.

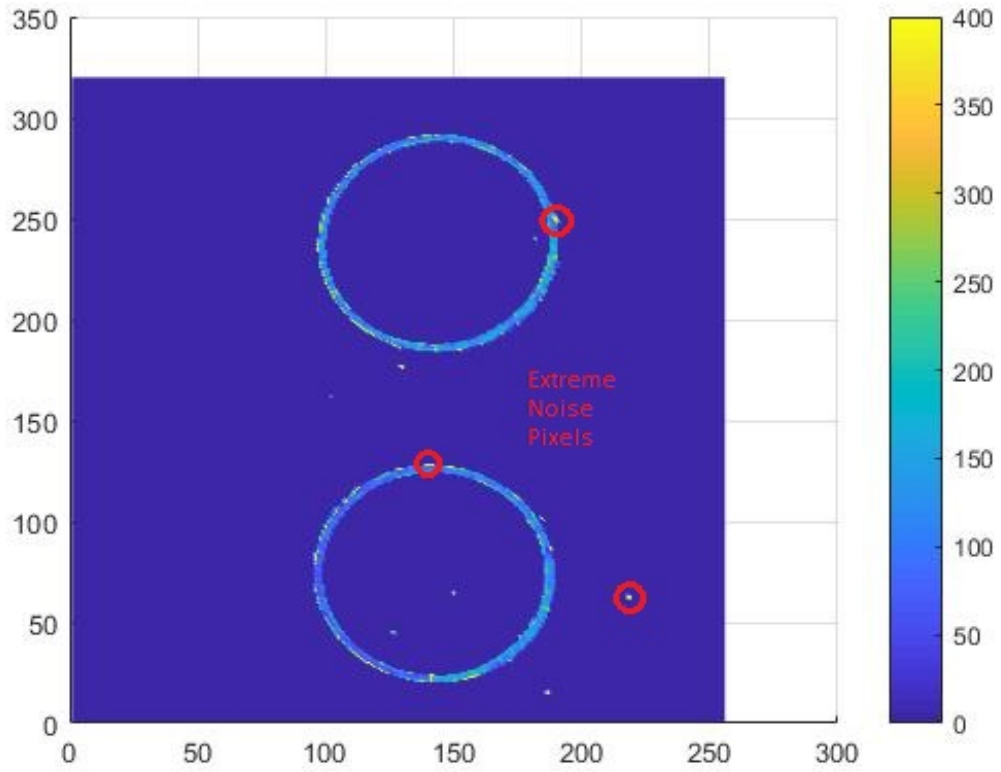

Figure 21. Image of the k-values immediately following a defect print before any noise reduction or Z-Calculation

Since the defect design pattern was not clearly visible, the first approach taken to reveal it was to separate the print into the known print quarters and attempt to determine if, despite the challenges of perceiving the variation visually, there was a variation that could be statistically determined. This approach employed the use of analysis of variance (anova) to determine if the populations were statistically different.

The goal was to observe a consistent trend (expected decrease counter-clockwise from the bottom) in the adjacent quarter's average k-values that matched the increasing skipping of layers. Anova plots from each quarter showed a statistically significant variation between them, but no consistent trend that matched the build pattern.

This approach produced a plot of the mean k-values with ninety-five percent confidence bars in order to visually determine any trend or separation, as seen in Figure 22. The goal was to see a consistent variation in the quarters values with distinct populations.

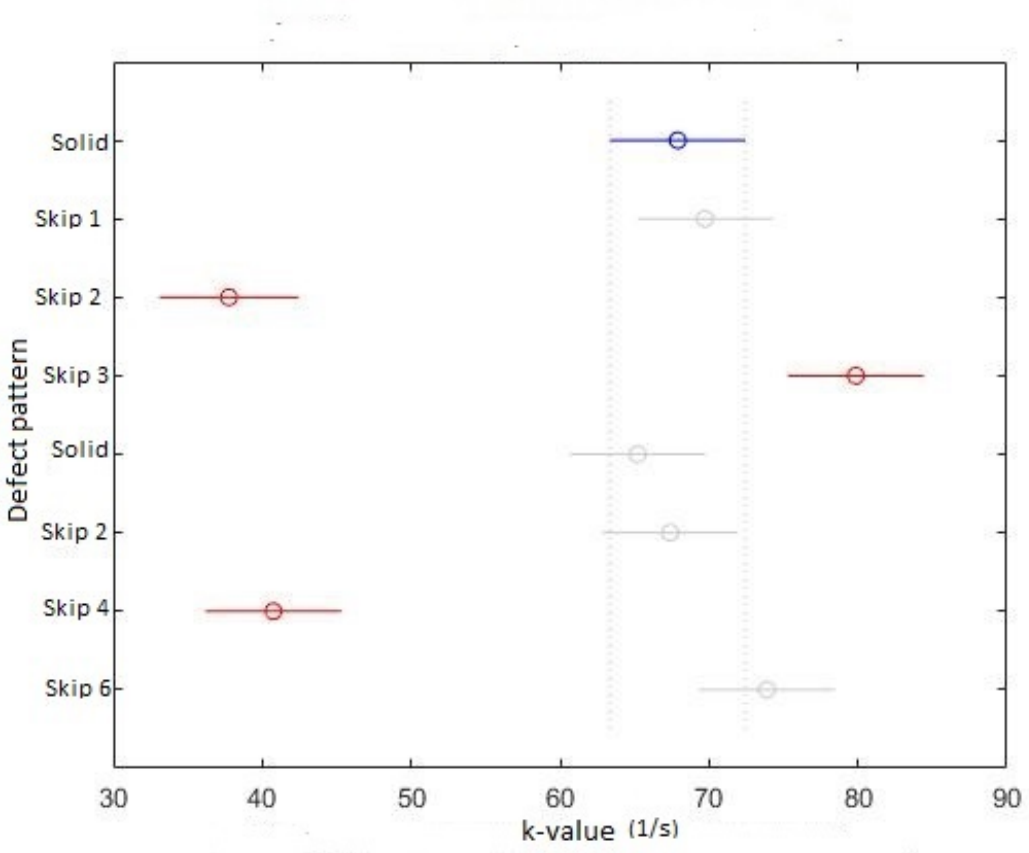

Figure 22. The average values of k for the quarters labeled on the Y axis with 95% confidence intervals. If there is an overlap between the selected quarter (in blue) and a given quarter, it is shown in grey. If not, it is red.

There were unique populations in the data as shown by the blue (separate by at least ninety five percent) versus grey (not separate by at least ninety five percent) with respect to the red section. The values were distributed around the ring but not related to the underlying pattern. This indicated that the distribution of the noise was inducing more consistent variation than the underlying defect pattern in this analysis. This approach was abandoned in favor of analyzing the entire frame of k-values, without separating it into defect quarters.

Statistically significant variation shown in Figure 22 in the quarter k-values was found even in the pre-defect layers. This indicated that the variation was likely inconsistent around the ring, but that inconsistency was consistent across layers. In order to reduce this variation, the data was normalized by the average values for each part of the print from the later pre-defect layers as there was no impact of the defect patterning for those layers. This approach successfully brought the data into a more homogeneous, overlapping confidence interval, population seen in Figure 23.

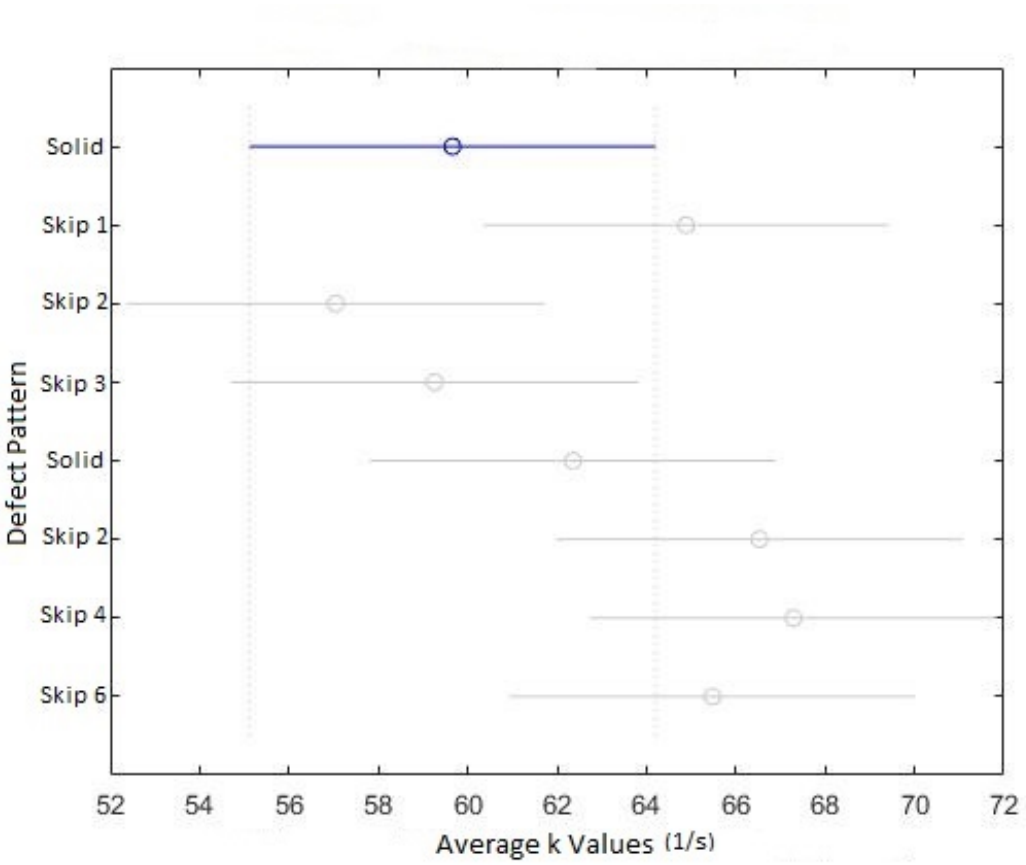

Figure 23. The normalized quarter averages based on the pre-defect layers. There is no visible pattern due to the variation in the data. Again, if there is an overlap between the selected quarter (in blue) and a given quarter, it is shown in grey. If not, it is red.

However, when the quarters with skipped layers were analyzed with this normalization, there was no consistent trend in the k-values and the variation between regions with different numbers of skipped layers was significantly less than the variation within each population of the same number of skipped layers. Additional attempts at reducing the noise by normalizing by the initial peak value and removing extreme k-values were performed, since there was no success in detecting the pattern via normalization.

Following these more computationally based approaches comparing quarters to

one another, a plot of the k-values for the entire print layer was again produced. At this point, the extreme variation in k-values between edge or spark pixels (upwards of 10,000) and normal print locations (approximately 150) was investigated to determine if there was a logical means of rejecting the extreme k-values. First, the k-values were given an upper bound of 400 in the fitting routine. This restriction limited the variation of values displayed in the plot to better show the fine variation between different defect quarters. Images before and after the limitation on the k-value are shown in Figure 24 and Figure 25 respectively. It did not yet elucidate the pattern but there is an improvement in the visualization of the data.

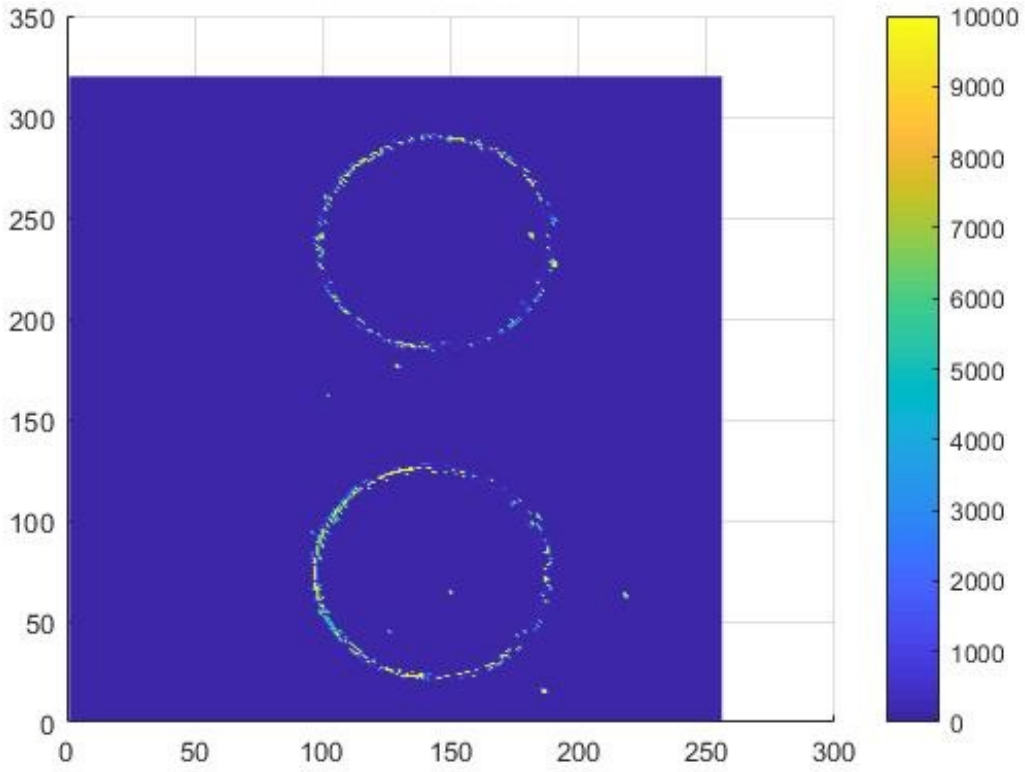

Figure 24. The pattern does not match the defect pattern and could not be elucidated due to the insurmountable variation in k-values.

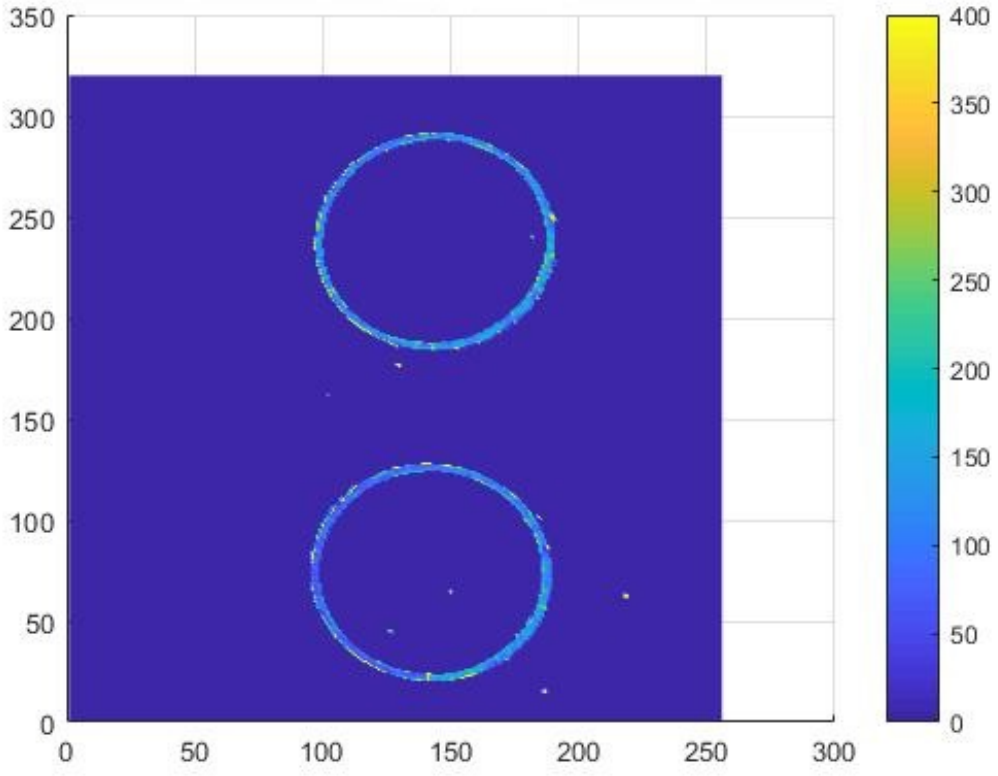

Figure 25. The pattern, although not immediately visible, was able to be elucidated by later data processing.

After the restriction in k-value, in order to logically separate the extreme data (non-print k-values) from the true data for print areas, Z score, the deviation from the mean in terms of standard deviations, was calculated as shown in Section 3.4 by the Equation 3. This Z score was then plotted and a more clearly visible variation could be seen in the true data under the noise after the values were normalized to the standard deviation seen in Figure 26.

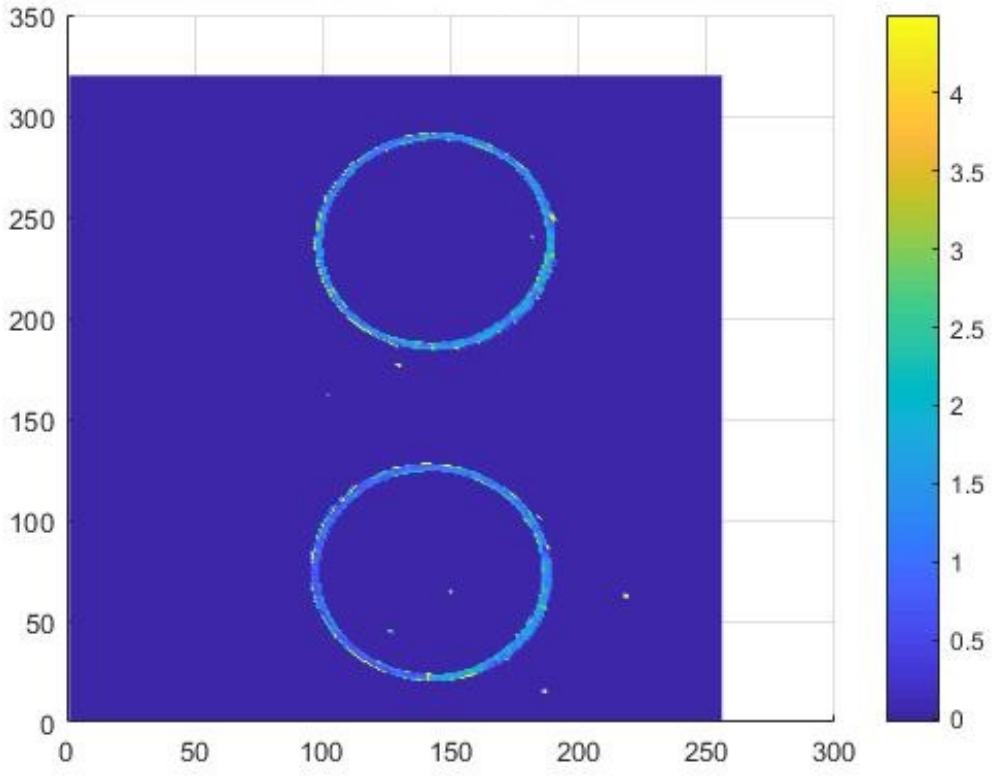

Figure 26. The values of the Z score calculated from the population of k-values for a layer immediately following a correctly printed defect set for the double skip ring on the bottom.

However, the extreme noise variation still obscured the variation due to defects between quarters and so cutoffs were set at a Z score of one and two standard deviations. The plot removing data outside one standard deviation was ineffective as shown in Figure 27. The image had many good data points removed. So, although an apparent pattern was visible, this pattern indicates the opposite of the expected trend.

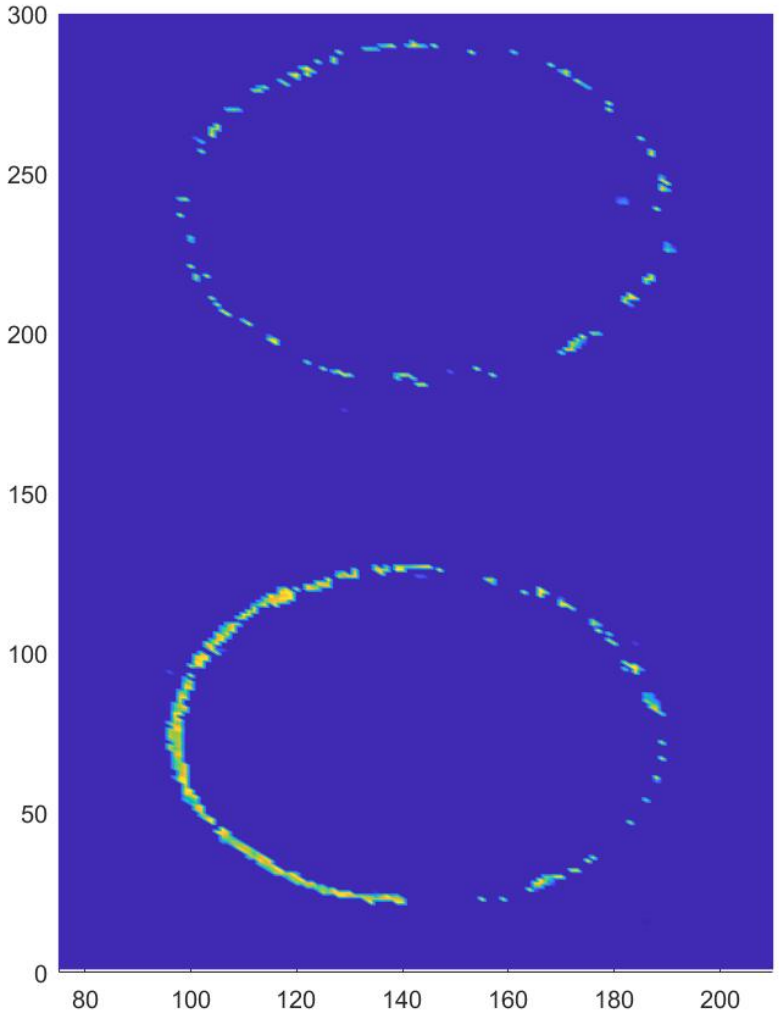

Figure 27. This figure shows only the points within one standard deviation of the mean k-values. As such, there were many points removed that were part of the normal variation. This made it difficult to observe the pattern.

So then a Z score of 2 was chosen. This removed only the k-values which were ninety seven percent or more likely to exist outside of the normally distributed data. The result, shown in 28 clearly shows a variation around the ring that matches the

expected trend of higher conduction near the solid portion and lower conduction proceeding around the ring as more underlying layers are skipped.

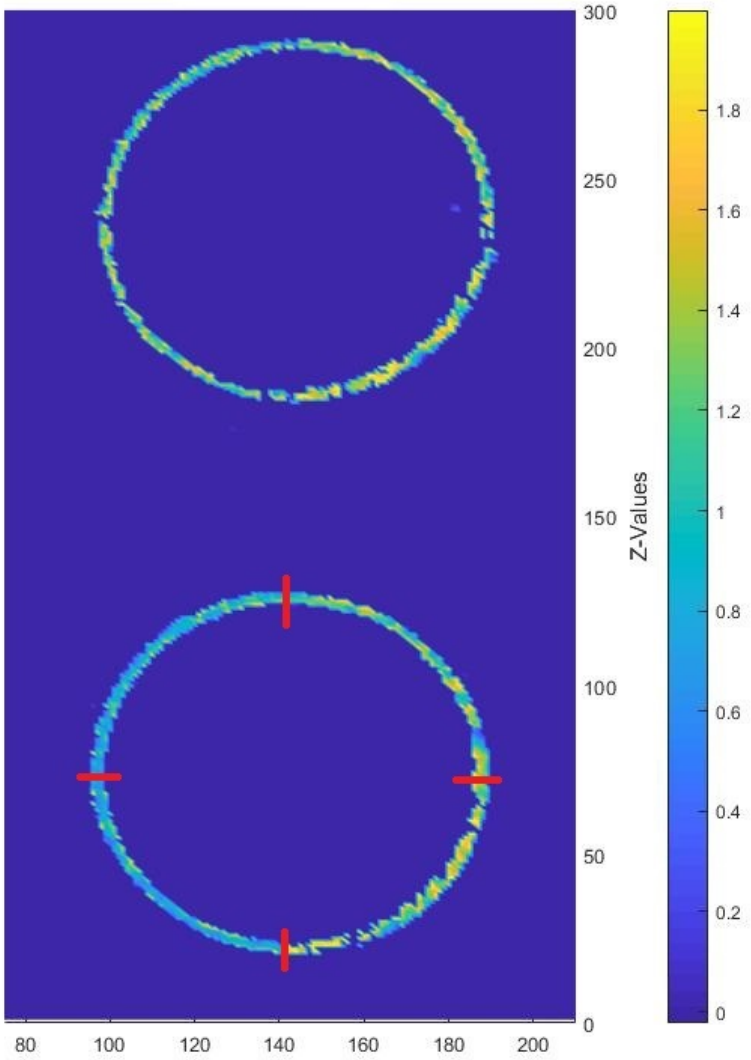

Figure 28. In the lower circle the defect print design can be seen as the gradient around the ring counter clockwise starting and ending at the lowest point in the circle. This is an image of the Z scores calculated from the k-values.

The pattern around the ring was more easily observed for the second print after enough layers to achieve layer separation. As discussed, the Z score was calculated and limited to plus and minus two, equivalent to 96% of the Gaussian probability density shown in Figure 29.

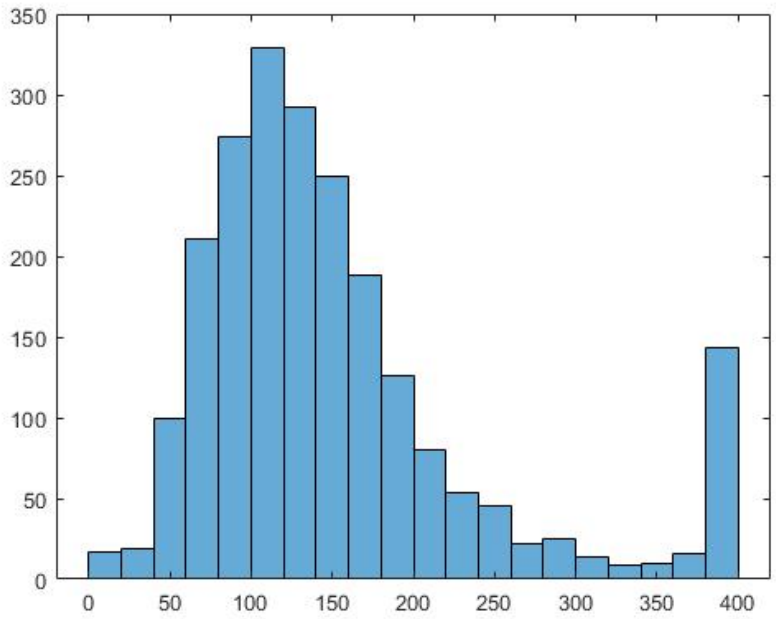

Figure 29. Z scores calculated from k-values for a post defect layer were used to reject all points more than 96% likely to fall outside of the normally distributed population. The mean of the k-values was found to be about 153 (1/s) for the chosen data set and the standard deviation approximately 89 (1/s) this data was captured of a print layer after a defect. This resulted in a cutoff that removed the large collection of values near 400 and gave a more normally distributed data set with an average near 116 (1/s).

After the noise pixels were eliminated, the average values and deviation for all of the parameters changed in addition to that of the k-value. The change to the variables can be seen in 2. The values were taken of a layer following a print defect.

	Avg w/o Removal	Avg w/Removal
A	2728 ± 1605	2975 ± 1583
k	153 ± 89	116 ± 51
C	346 ± 188	331 ± 177
D	$.386 \pm .267$	$.416 \pm .281$
E	152 ± 277	158 ± 284

Table 2. Average and standard deviation values for all the model variables before and after the Z score elimination. This data is of a layer immediately following a print defect.

Additionally, the noise was much higher for the second print and the regions where the printer is printing directly onto unmelted powder tend to have much higher rates of spatter and denudation effects. The pattern is shown in Figure 30. The ring in the bottom left is the ring of interest because it produced a solid geometry with separation at the defect layers.

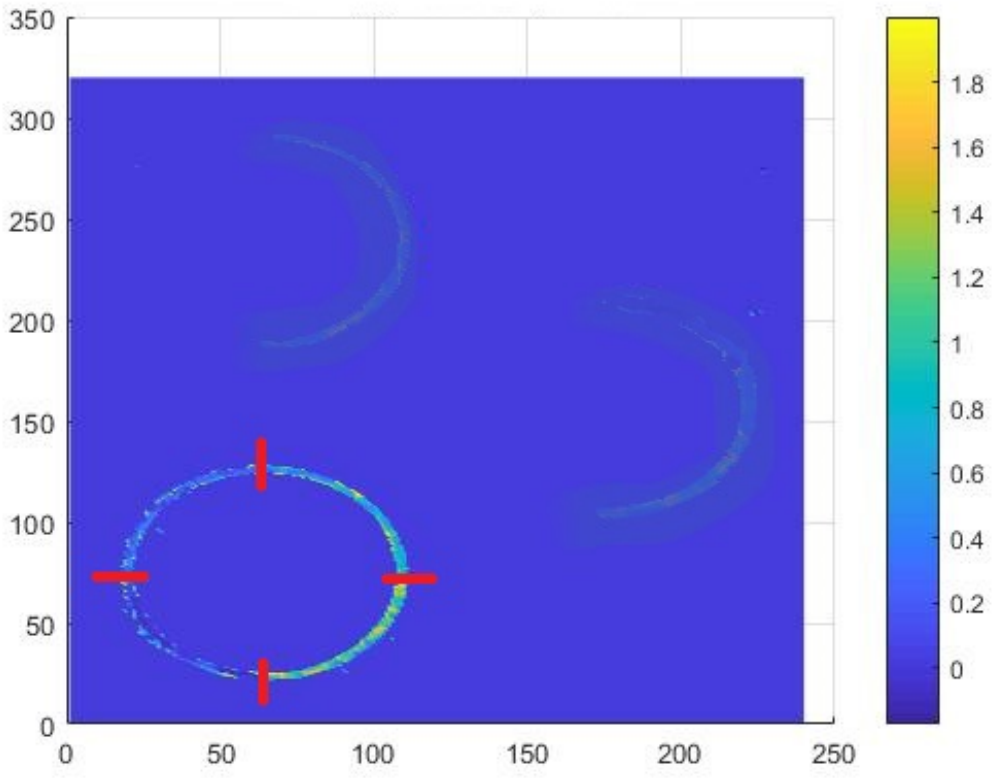

Figure 30. Z scores calculated from k-values for a post defect layer in the bottom left ring for the 0/5/10/15 pattern moving counter clockwise around the ring from the bottom.

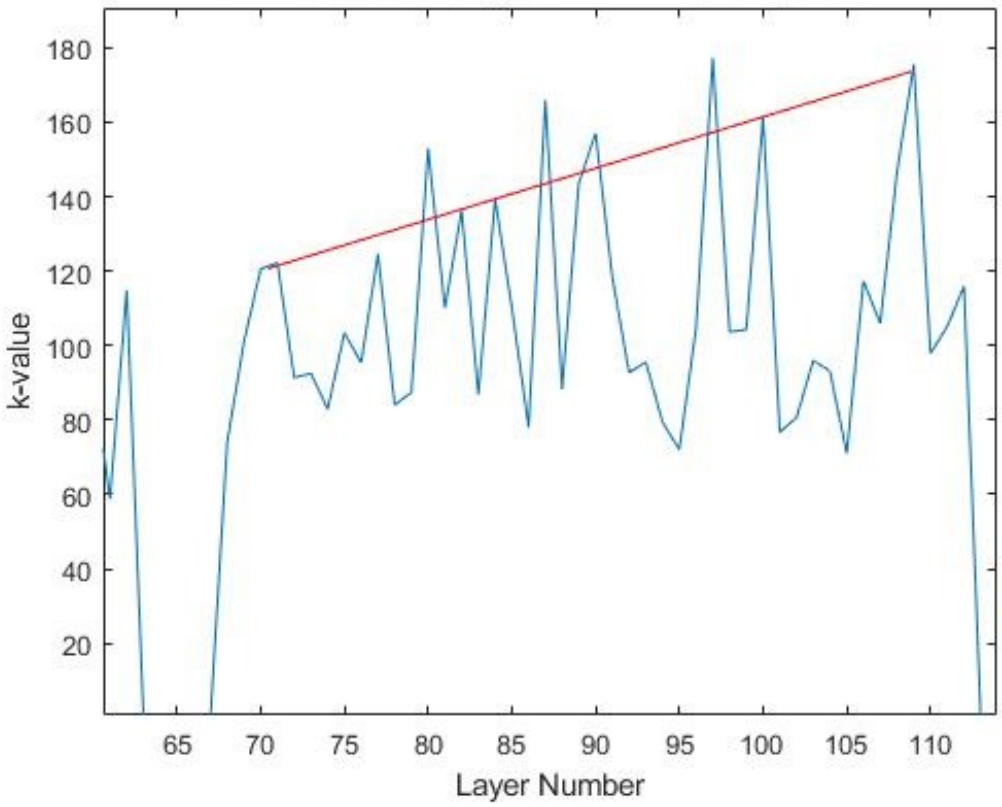

Figure 31. The k-value for a pixel was tracked in the layers during and after a defect print. This shows the zero values for the layers where nothing was printed. After the defect, the k-value steadily increases till it reaches nominal cooling behavior.

The observed decrease in k-value returns to nominal as the subsequent layers are printed above the defect shown in Figure 31. For the most distinct pattern (lower left ring) in Figure 30, the pattern disappears, even with noise reduction, after about twenty layers. The pattern eventually returns to mostly nominally equal cooling around the ring, as seen in Figure 32. This is a much greater persistence than the prints with fewer skipped layers which persisted only for a couple of layers. This is likely due to achieving true separation, since in the first print's first non-defect layer melted and fused all the skipped layers to the solid underneath.

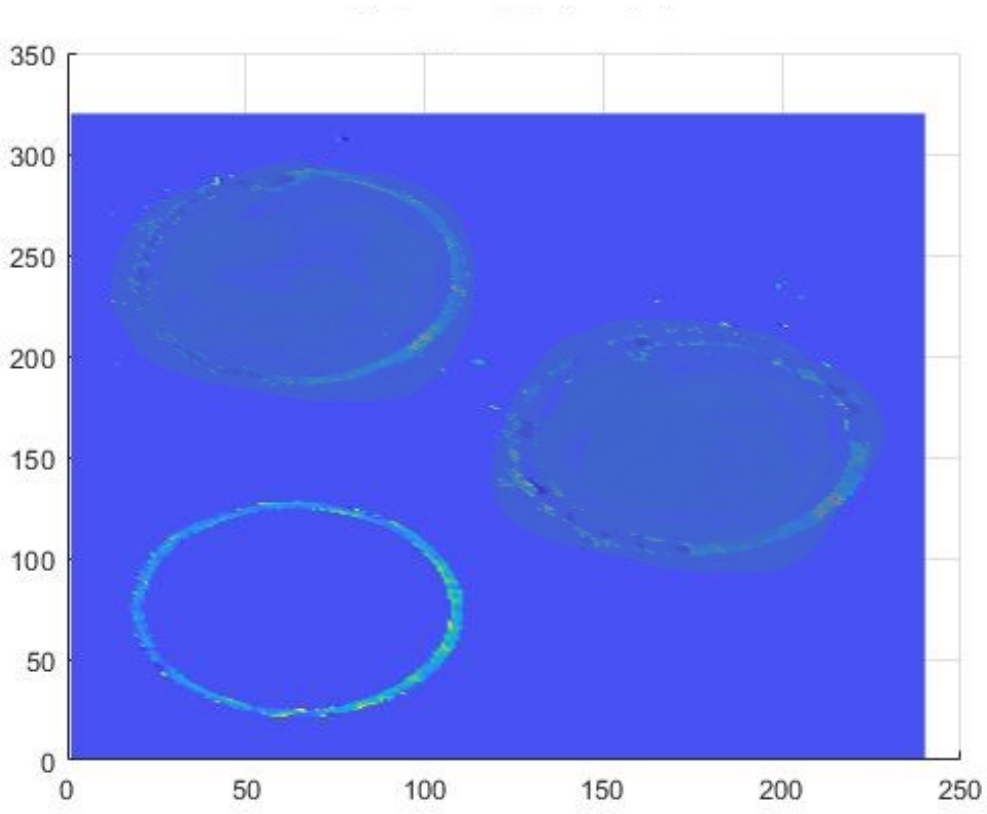

Figure 32. Z scores calculated from k-values for a post defect layer after twenty layers have been printed above the lower left hand circle. This shows that the cooling becomes nominally equal around the ring before the next print starts.

4.4 Scanning Electron Microscopy

4.4.1 Preparation

In order to better understand the kind of defects that the k-value change can detect, the samples from the first print (one to six skipped layers) were prepared for inspection using Scanning Electron Microscopy (SEM). SEM is the process of restoring the sample with a focused beam of electrons and collecting the scattered electrons from the sample to generate an image. This provides high resolution imagery

on the micrometer scale. The printed rings were sectioned within each defect quadrant and mounting using metal coils that held the sample in place while it was mounted in a thermoset plastic puck. The puck is then easier to secure while the cut edge is ground and polished. The thermoset provides the black background in the images. The grey material is the printed metal and the subject of interest in the images.

4.4.2 Findings

Some degree of unmelted or undermelted powder leading to a void at the location of the defect layers was expected. Instead of the expected gap, we found the shape in Figure 33.

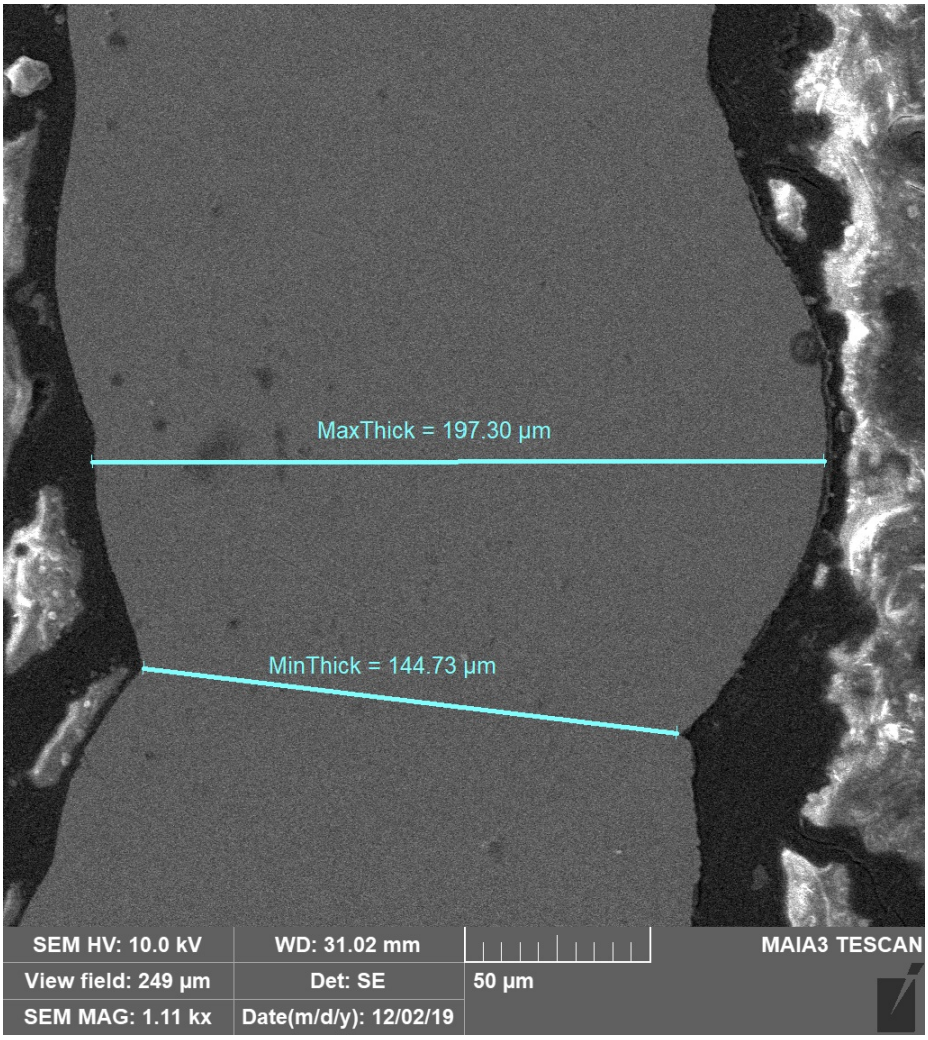

Figure 33. Defects produced by skipping pattern were periodic thinning and bulges instead of voids. The normal thickness of the wall was found to be about 180 μm.

A slimmer portion of wall followed by a bulge was found at the location of each defect. The location of each defect was determined from the SEM imagery. The distance between the bulges was measured and it was found to match the number of layers (nineteen for this image) and the 30 μm layer height, as shown in Figure 34.

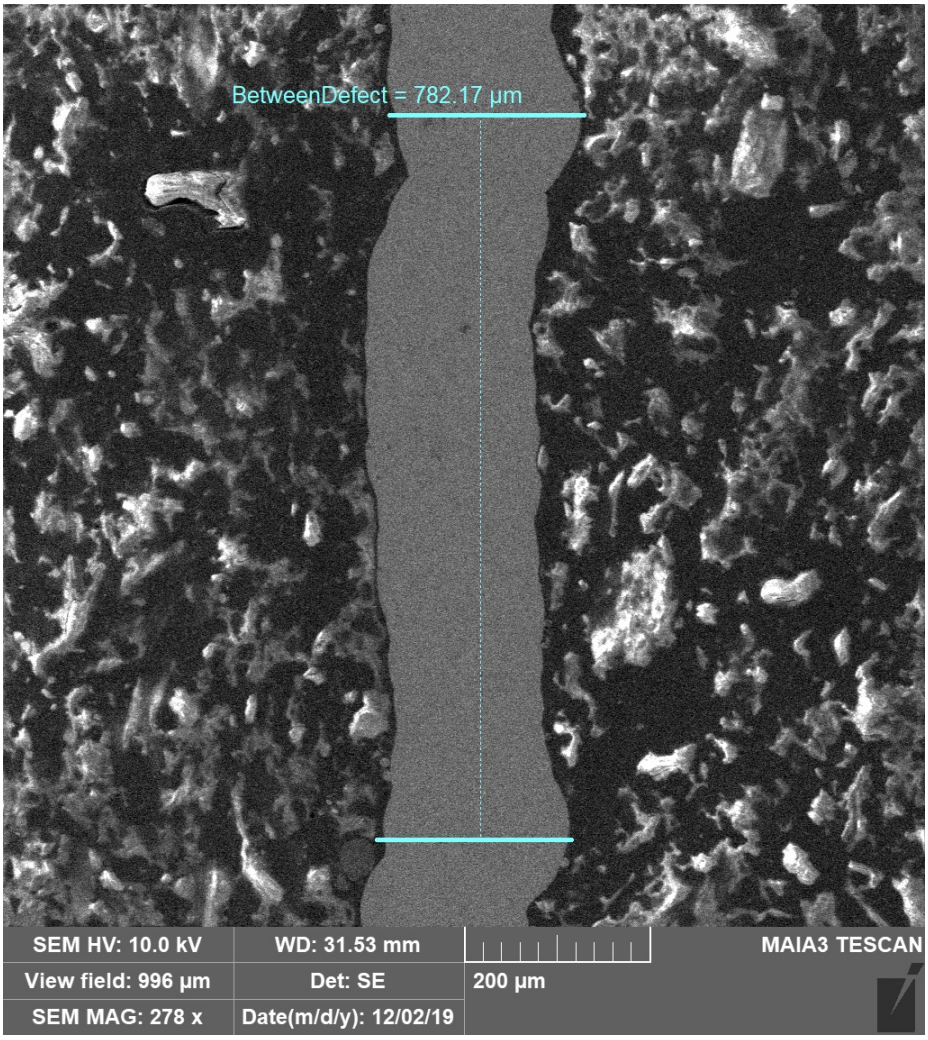

Figure 34. Spacing of defects matches the calculated 19 layers with 30 μm layer thickness.

Reduction of wall thickness does decrease the conductivity to the build plate [26]. However, this effect is significantly less than the effect of a void at the same location because the conductivity of the unmelted powder is approximately equivalent to open air. This demonstrates the sensitivity of this method. If it is capable of detecting a change in wall thickness of about twenty five percent, then it would be expected to be capable of detecting more significant reductions in conductivity due to underlying voids. Additionally, this sensitivity indicates that this method may be able to detect

the true wild type defects which have smaller impacts on wall conductivity than a full void.

The cause of this defect structure instead of true voids is suggested by some previous work manufacturing fine holes in LPBF manufactured parts [2, 4]. When small holes (consisting of five to about thirty five layers) were printed, the laser tracks printed above the hole over-melted and resealed the hole or created an incorrect, compressed geometry. The laser is designed to melt beyond the surface layer of powder in order to induce better cohesion between layers. However, when building thin walled structures over powder, it may become necessary to either decrease the laser power or to engineer with the over-melting in mind. The lack of true voids in our defects was unexpected, but increased confidence in the sensitivity of our model.

V. Conclusions

The goal of this research was to develop an in-situ monitoring process for LPBF-AM processes. To that end, an approach using active collection of IR emission for each laser pass and its respective cool down was developed and tested. The system detected the reduced cooling rate for programmed anomalous print behavior used as an analogue to printing errors. The part geometry tested was representative of a thin walled structure. For these geometries, the system was capable of detecting the changed conductivity for all of the programmed layer skip defects.

5.1 Trend in Conductivity

Layer skip defects do not represent the common defect structures such as keyhole defects, lack of fusion defects or other pores. Instead, they more accurately resemble the effect of printing a small hole which is over melted and resealed by the layers above, an effect that has been investigated in prior research [4]. This defect often presents as a bulb of thicker material and a thinner connection where it has been fused to the layers below incompletely. This means that the conduction pathway is restricted, but not cut off. So the effects on conduction are less pronounced. Due to the thermal resistance of voids, it can be expected that any observed effect on the conduction would only be more pronounced for voids formed by lack of fusion or keyhole defects than for minor variations in wall thickness.

Despite the unnatural defect generation, there is a marked trend in the k-values around the defect print that indicates the change in conductive behavior as seen in Figure 35. The trend around the ring matches the expected reduction in conduction as a greater number of layers were skipped.

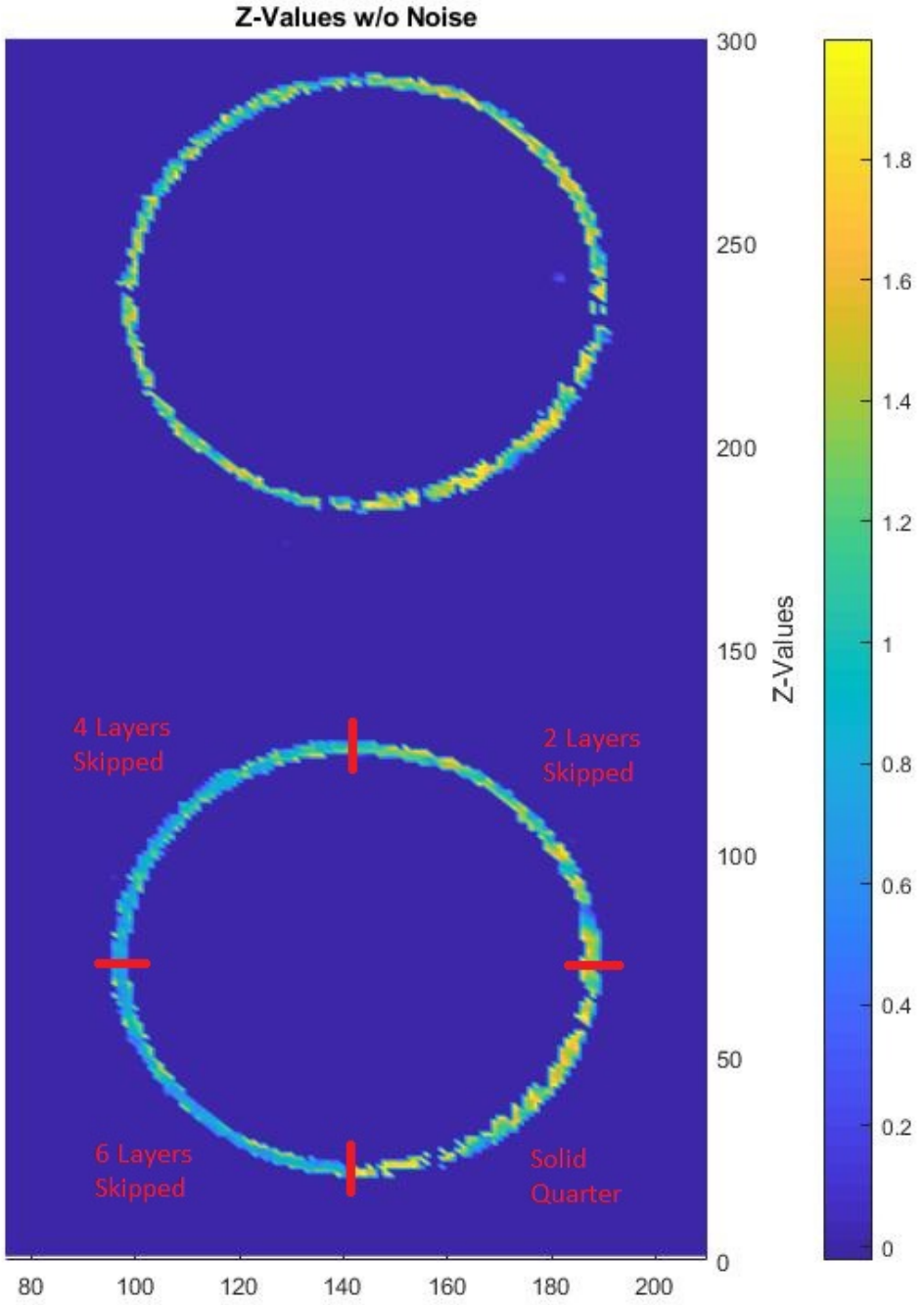

Figure 35. The trend in the Z-values that matches the pattern of defect print on the lower ring. The upper ring is separated from its much smaller defect design by a number of layers so its pattern is not visible.

This method makes a significant step toward actively monitoring the print, but does not represent a complete monitoring system in and of itself. As discussed previously in Section 2.5, active monitoring requires that the system be able to make adjustments to the print in real time. The hindrances of calibration, data volume, noise, and printer integration still apply, but this approach is simpler to process and the infrastructure exists to actively sense the field of view of the print area. This method advanced the field by addressing the limitations by avoiding calibration and reducing noise. Data transfer and processing can be performed rapidly with future system design and optimization. All that remains to use this system for monitoring instead of simply sensing is to establish correction criteria to integrate into the printing process. However, these will be built over time by experience and experimentation as the exact signature of different defect types are identified in terms of the k-value.

5.2 Limitations

In order to assess the k-value as a potential indicator of part quality, a number of steps were taken to increase the ability of detecting any correlation. The most natural experiment would be to look for potential defects with this approach and later section the part to determine if regions of anomalous cooling or k-value correlate with real physical defects. This would be the most complete determination of whether or not the parameter accurately detects defects. However, sectioning the final print and grinding to the exact layer containing a potential random defect would be very difficult. The parameter was investigated first to determine if it was an appropriate analogue for conduction and if it was indicative of a print defect. Synthetic conditions were chosen to create print defects at known locations increasing the chance of detecting variation in conductivity between induced defects and non-defect areas.

Then choices were made to evaluate the basic viability of this method. This helped defects to be easily found but limited the scope of our results.

The defect design was described in Section 3.3. Because the design defects were large to make them easily defined and not designed to be random or naturally occurring, this work did not evaluate the spacial resolution of the technique or the minimum detectable defect size. The resolution is fundamentally limited by the camera viewing angle and pixel resolution which was about 240 μm. If the defect is smaller than a pixel, its exact location will be unknown and it could even be obscured by the good print locations within the same pixel. The only indication of sensitivity determined here is that the method was able to detect the reduction in conduction pathway, wall thickness, produced by the design defects. However, this does not indicate the detection limits of this method to small defects.

Another limitation of our investigation was the printing of thin walled structures only. This is not a critical limitation, as thin structures are common in AM parts. The primary reason our investigation was limited to these structures was to magnify small differences in conduction pathways from the surface. Additionally, it is more difficult to observe the entire cooling process when a part is being constructed in bulk due to the repeated reheating of the scanning pattern. This decreases the amount of data to be separated, and so thin walled, single pass structures were chosen for this proof of concept.

We also limited our scope to appropriately scale our research goals. The greater research question is whether an active monitoring system for LPBF-AM is achievable, and if so, what is the best approach. Many approaches have been tried. Our goal was to propose and perform initial tests on an intermediate complexity parameter, between maximum temperature and precise conduction, that could potentially be utilized to detect print defects. Because of this, the processing and analysis was

all done after the print. There are a number of challenges, specifically data volume and printer integration, to active monitoring that we have not attempted to address. The necessity of post-processing is largely due to the data transfer from camera, to controlling computer, and finally to the analysis computer. This limited the scope of the capabilities we have tested with the system.

The next challenge was the wide range of deviation in the normal cool-down behavior. The standard deviation seen in normal good prints was so high, the variation due to the defects was more difficult to see. After removing extreme data values, the standard deviation of remaining data was reduced enough to detect the induced defects. However, the source of the extreme deviation could not be completely attributed to sources in the measurement or printing. As a result, they may or may not be consistent if replicated elsewhere. This is why rather than attempting to find the source of the deviation, the decision was made to account for it computationally through the Z score and view the data in such a manner that it would be seen through. This deviation will need to be better characterized in order to develop more automatic monitoring; however, that is beyond the scope of our research goals.

5.3 Advantages

There are a number of advantages of this system over previous sensing methods. Two of the benefits are the flexibility and simplicity of this method.

One such advantage is that this method is independent of knowledge of the material being printed and does not need to be altered for differing alloys that could be used in LPBF. This is advantage becomes more significant as the field of available alloys is expanding rapidly and already is very diverse. In order to use some of the more complex monitoring methods previously investigated by others, it would be necessary to conduct significant material testing or obtain detailed material properties on

new alloys. For example, methods that attempt to correlate IR emission to absolute temperature require knowledge of the material's emissivity over the relevant range of temperatures and wavelengths.

Another advantage is that, imaging the relative value at each layer does not require any knowledge of the laser path as long as the part is in the field of view or a computational thermal model of the part to compare to calculated values. This increases the flexibility of this method and would ideally allow the analysis to be general enough that it could be used on any print geometry. The current analysis could be performed on any thin walled component similar to those discussed here without prior knowledge of the specific design or shape.

The final benefit was not realized in this work. However, the IR imagery is captured in real time and the analysis is designed to be simplistic enough that the the data processing could potentially be conducted within the time for the printer to reset for the next print layer. The largest barrier to real time sensing currently is data transfer. The existing data transfer mechanisms available with the camera and control computer are not capable of transferring the data collected to allow real-time analysis. However, should this problem be resolved,perhaps through on camera processing or faster data communications, this method of data collection and processing is rapid enough to achieve active sensing.

5.4 Intermediate Findings

In the process of developing the monitoring method discussed above, observations were made which reinforced the usefulness of this method and a key assumption in the field. The quantification of the reduction in conduction as distance from the build plate increased shown in Figure 15. This reduction has been widely assumed and has led to the common practice of adding additional layers to the beginning of

prints that are later removed, but the reduction date and necessary number of layers is not commonly reported. The trend is graphically shown in the change in average conduction constant as a function of build height in Figure 15. The conduction constant decreases linearly before leveling off after approximately 50 layers at a 10% decrease. There is general agreement that conduction decreases with distance from the build plate till it reaches a steady state. The conduction parameter developed here also follows this trend and supports the theory that the k-value is an appropriate analogue for the conduction in a sample.

5.5 Future Work

Future investigations inspired by this research in LPBF AM are broken into a few categories. Detailed analysis of the k-value's model and effectiveness must be completed to ensure that this term is as powerful as early indications show. Additionally, there are many obstacles impeding its application, so research to improve the apparatus as a whole is necessary. Finally, during this project a number of interesting trends emerged which would could be investigated with additional prints.

It would be highly beneficial to calculate the k-value alongside some of the more complex conduction models such as those used by Krauss [9]. Alternatively, an even simpler approach could be explored such as performing a two point analysis of the initial intensity to the intensity after a characteristic time. Another approach would be to improve the existing model and method.

The modelling equation should be further improved and iterated. The model was constructed to represent the three distinct regions visible in the cooling curve. These are broken into a rapid decrease followed by a transition period to a slow decrease. Each region is closely linked to a term in the modeling equation. However, the equation is made of approximations of the heat transfer equations. Further modifications

and adaptations of this model can make these approximations more realistic. For example, it seems that the radiative term could be better described since the D term has a strong correlation to the other constants. Also, there may be alternate functional forms which would not over-complicate the model. The model used was effective and could serve as a basis for further investigation.

As previously discussed, this approach is not yet an active monitoring method. More work needs to be done to integrate the calculations into the camera, provide a usable output, and further automate the system. This could be approached by either improving the software, hardware, or data transfer mechanism. Regardless of how they are approached, these steps are not trivial, but realistically possible due to the relative simplicity of the calculations being performed. Additionally, decisions must be made as to how the output will be used. It must be decided how much human oversight to provide, the level of confidence in the method, and any redundant inspection that may be incorporated.

This method should be investigated in conjunction with other means of quality control. Having redundant layers of inspection can increase the sensitivity or cover different defect scenarios. It is in the best interest of LPBF-AM as a field to present and investigate as many NDE techniques as possible to give the greatest diversity of options to the customer. With more options, the technique can be tailored to the situation and levels of confidence can be established. Through the improvement of the model and system, this method can potentially provide confidence in the quality of LPBF-AM components, perhaps rising to the level of other traditionally manufactured parts.

Utilizing further prints, the investigation of the k-value must be expanded beyond one alloy and a couple of designs. The reproducability and consistency of the parameter must be investigated in different geometries and materials. Thick components

provide many challenges such as redundant cooling pathways, rapid reheating of the print through the hatch pattern, and larger relevant data volumes. Currently, the parameter is highly effective in thin walled structures partially due to the geometry. For these reasons, there should be subsequent investigations as to whether the usefulness of this parameter is limited or more broadly applicable.

A number of research gaps presented themselves in the process of developing the k-value parameter that were unrelated to the particular development of this system, but represent potential areas of future research and prints. One such area is an expansion of the quantitative analysis of the effect on conduction of distance from the build plate performed in this study to include more alloys and build parameters. This would allow for a clear understanding of how the distance from the plate impacts the build and help prescribe how many extra layers are required to reduce waste. Another area of interest is a detailed investigation of the overmelting behavior of the chosen laser parameters. If, when designing a part, the technician understood exactly under what conditions and how deep the laser would overmelt then the part could be engineered to produce a more correct geometry. These areas are critical to LPBF AM but are not directly connected to the further investigation of k-value.

Finally, in future prints, an in-depth analysis of the k-value's ability to detect various forms of naturally occurring defects must be performed. This should include random induction of defects by detuning the laser scan speed and power for the purpose of producing keyhole and lack of fusion defects to determine statistical capability and the sensitivity of this method. The other necessary step to bring the k-value closer to reality would be to apply the test to bulk structures and more complex printing geometries. The simplistic approach was appropriate for a proof of concept, but does not represent realistic printing scenarios.

5.6 Contributions

The decrease in measured k-value around the printed ring, in combination indicate that the k-value serves as an effective indicator of the conduction from the surface for a given point. Conduction is known to be effected by the presence of underlying voids [9]. The effectiveness and sensitivity of this approach, combined with the simplicity of calculation makes this conductive term a promising thermal parameter to observe as a means of monitoring underlying part quality. Additionally, the simplicity and sensitivity make this sensing method a viable part of an active monitoring system for LPBF AM.

Bibliography

1. Grasso, M. and Colosimo, B. M., "Process Defects and In Situ Monitoring Methods in Metal Powder Bed Fusion: A Review," *Measurement Science and Technology*, Vol. 28, No. 4, apr 2017.

2. Hassanin, H., Finet, L., Cox, S. C., Jamshidi, P., Grover, L. M., Shepherd, D. E., Addison, O., and Attallah, M. M., "Tailoring Selective Laser Melting Process for Titanium Drug-Delivering Implants with Releasing Micro-Channels," *Additive Manufacturing*, Vol. 20, mar 2018, pp. 144–155.

3. Kenney, M. E., "Cost Reduction Through the Use of Additive Manufacturing (3D Printing) and Collaborative Product Lifecycle Management Technologies to Enhance the Navy's Maintenance Programs," *Acquisition Research Program Sponsored Report Series*, 2013.

4. Solyaev, Y., Rabinskiy, L., and Tokmakov, D., "Overmelting and Closing of Thin Horizontal Channels in AlSi10Mg Samples Obtained by Selective Laser Melting," *Additive Manufacturing*, Vol. 30, dec 2019, pp. 100847.

5. Bremen, S., Meiners, W., and Diatlov, A., "Selective Laser Melting," *Laser Technik Journal*, Vol. 9, No. 2, apr 2012, pp. 33–38.

6. Martin, J. H., Yahata, B. D., Hundley, J. M., Mayer, J. A., Schaedler, T. A., and Pollock, T. M., "3D printing of high-strength aluminium alloys," *Nature*, Vol. 549, No. 7672, sep 2017, pp. 365–369.

7. Newell, D. J., O'Hara, R. P., Cobb, G. R., Palazotto, A. N., Kirka, M. M., Burggraf, L. W., and Hess, J. A., "Mitigation of scan strategy effects and material anisotropy through supersolvus annealing in LPBF IN718," *Materials Science and Engineering A*, 2019.

8. Grasso, M., Laguzza, V., Semeraro, Q., and Colosimo, B. M., "In-Process Monitoring of Selective Laser Melting: Spatial Detection of Defects Via Image Data Analysis," *Journal of Manufacturing Science and Engineering*, Vol. 139, No. 5, may 2017, pp. 051001.

9. Krauss, H., Zeugner, T., and Zaeh, M. F., "Layerwise Monitoring of the Selective Laser Melting Process by Thermography," *Physics Procedia*, Vol. 56, 2014, pp. 64–71.

10. Hirsch, M., Patel, R., Li, W., Guan, G., Leach, R. K., Sharples, S. D., and Clare, A. T., "Assessing the Capability of In-Situ Nondestructive Analysis During Layer Based Additive Manufacture," *Additive Manufacturing*, Vol. 13, jan 2017, pp. 135–142.

11. Ibrahim, K. A., Wu, B., and Brandon, N. P., "Electrical Conductivity and Porosity in Stainless Steel 316L Scaffolds for Electrochemical Devices Fabricated using Selective Laser Sintering," *Materials and Design*, Vol. 106, sep 2016, pp. 51–59.

12. Gusarov, A., Yadroitsev, I., Bertrand, P., and Smurov, I., "Heat Transfer Modelling and Stability Analysis of Selective Laser Melting," *Applied Surface Science*, Vol. 254, No. 4, dec 2007, pp. 975–979.

13. Gusarov, A. and Smurov, I., "Modeling the Interaction of Laser Radiation with Powder Bed at Selective Laser Melting," *Physics Procedia*, Vol. 5, No. PART 2, 2010, pp. 381–394.

14. Bidare, P., Bitharas, I., Ward, R., Attallah, M., and Moore, A., "Fluid and Particle Dynamics in Laser Powder Bed Fusion," *Acta Materialia*, Vol. 142, jan 2018, pp. 107–120.

15. Gong, H., *Generation and detection of defects in metallic parts fabricated by selective laser melting and electron beam melting and their effects on mechanical properties.*, Ph.D. thesis, University of Louisville, 2013.

16. Hooper, P. A., "Melt Pool Temperature and Cooling Rates in Laser Powder Bed Fusion," *Additive Manufacturing*, Vol. 22, No. May, aug 2018, pp. 548–559.

17. Maamoun, A. H., Xue, Y. F., Elbestawi, M. A., and Veldhuis, S. C., "Effect of Selective Laser Melting Process Parameters on the Quality of Al Alloy Parts: Powder Characterization, Density, Surface Roughness, and Dimensional Accuracy," *Materials*, Vol. 11, No. 12, nov 2018, pp. 2343.

18. Bartlett, J. L., Heim, F. M., Murty, Y. V., and Li, X., "In Situ Defect Detection in Selective Laser Melting via Full-Field Infrared Thermography," *Additive Manufacturing*, Vol. 24, No. December, dec 2018, pp. 595–605.

19. Taheri Andani, M., Dehghani, R., Karamooz-Ravari, M. R., Mirzaeifar, R., and Ni, J., "A Study on the Effect of Energy Input on Spatter Particles Creation During Selective Laser Melting Process," *Additive Manufacturing*, Vol. 20, mar 2018, pp. 33–43.

20. Kanko, J. A., Sibley, A. P., and Fraser, J. M., "In Situ Morphology-Based Defect Detection of Selective Laser Melting through Inline Coherent Imaging," *Journal of Materials Processing Technology*, Vol. 231, may 2016, pp. 488–500.

21. Coeck, S., Bisht, M., Plas, J., and Verbist, F., "Prediction of Lack of Fusion Porosity in Selective Laser Melting Based on Melt Pool Monitoring Data," *Additive Manufacturing*, Vol. 25, jan 2019, pp. 347–356.

22. Scime, L. and Beuth, J., "Using Machine Learning to Identify In-Situ Melt Pool Signatures Indicative of Flaw Formation in a Laser Powder Bed Fusion Additive Manufacturing Process," *Additive Manufacturing*, Vol. 25, jan 2019, pp. 151–165.

23. Craeghs, T., Clijsters, S., Kruth, J.-P., Bechmann, F., and Ebert, M.-C., "Detection of Process Failures in Layerwise Laser Melting with Optical Process Monitoring," *Physics Procedia*, Vol. 39, 2012, pp. 753–759.

24. Mahmoudi, M., Ezzat, A. A., and Elwany, A., "Layerwise Anomaly Detection in Laser Powder-Bed Fusion Metal Additive Manufacturing," *Journal of Manufacturing Science and Engineering*, Vol. 141, No. 3, mar 2019, pp. 031002.

25. Imani, F., Gaikwad, A., Montazeri, M., Rao, P., Yang, H., and Reutzel, E., "Process Mapping and In-Process Monitoring of Porosity in Laser Powder Bed Fusion Using Layerwise Optical Imaging," *Journal of Manufacturing Science and Engineering*, Vol. 140, No. 10, oct 2018, pp. 101009.

26. Schilp, J., Seidel, C., Krauss, H., and Weirather, J., "Investigations on Temperature Fields during Laser Beam Melting by Means of Process Monitoring and Multiscale Process Modelling," *Advances in Mechanical Engineering*, Vol. 6, jan 2014, pp. 217584.

27. Grasso, M., Gallina, F., and Colosimo, B. M., "Data Fusion Methods for Statistical Process Monitoring and Quality Characterization in Metal Additive Manufacturing," *Procedia CIRP*, Vol. 75, 2018, pp. 103–107.

REPORT DOCUMENTATION PAGE

Form Approved
OMB No. 0704–0188

1. REPORT DATE *(DD–MM–YYYY)*	2. REPORT TYPE	3. DATES COVERED *(From — To)*
03-26-2020	Master's Thesis	Sept 2018 — Mar 2020

4. TITLE AND SUBTITLE

Conduction Mapping for Quality Control of Laser Powder Bed Fusion Additive Manufacturing

5a. CONTRACT NUMBER

5b. GRANT NUMBER

5c. PROGRAM ELEMENT NUMBER

6. AUTHOR(S)

Baxter, Chance M, 2d Lt

5d. PROJECT NUMBER

5e. TASK NUMBER

5f. WORK UNIT NUMBER

7. PERFORMING ORGANIZATION NAME(S) AND ADDRESS(ES)

Air Force Institute of Technology
Graduate School of Engineering and Management (AFIT/EN)
2950 Hobson Way
WPAFB OH 45433-7765

8. PERFORMING ORGANIZATION REPORT NUMBER

AFIT-ENP-MS-20-M-080

9. SPONSORING / MONITORING AGENCY NAME(S) AND ADDRESS(ES)

Intentionally left blank

10. SPONSOR/MONITOR'S ACRONYM(S)

N/A

11. SPONSOR/MONITOR'S REPORT NUMBER(S)

12. DISTRIBUTION / AVAILABILITY STATEMENT

DISTRIBUTION STATEMENT A:
APPROVED FOR PUBLIC RELEASE; DISTRIBUTION UNLIMITED.

13. SUPPLEMENTARY NOTES

14. ABSTRACT

A process was developed to identify potential defects in previous layers of Selective Laser Melting (SLM) Powder Bed Fusion (PBF) 3D printed metal parts using a mid-IR thermal camera to track infrared 3.8-4 μm band emission over time as the part cooled to ambient temperature. Efforts focused on identifying anomalies in thermal conduction. To simplify the approach and reduce the need for significant computation, no attempts were made to calibrate measured intensity, extract surface temperature, apply machine learning, or compare measured cool-down behavior to computer model predictions. Raw intensity cool-down curves were fit to a simplified functional form designed to approximate the behavior of radiative, conductive, and convective heat transfer, yielding a conductivity parameter. This parameter was able to identify minor changes, less than twenty five percent, in the thickness of a single layer of the walls of single-pass, thin-wall structures and the presence of underlying unfused powder. Small voids were not produced in the test prints analyzed here. The thermal signature of underlying fusion defects, as measured by the conductivity parameter, is clearly present for many layers. This method was shown to be effective in detecting changes in conductivity of the material which represents a large portion of the defects commonly found in SLM additive manufacturing.

15. SUBJECT TERMS

LPBF, Quality Control, Infrared Imagery, 3D Printing

16. SECURITY CLASSIFICATION OF:			17. LIMITATION OF ABSTRACT	18. NUMBER OF PAGES	19a. NAME OF RESPONSIBLE PERSON
a. REPORT	b. ABSTRACT	c. THIS PAGE			Maj Nicholas Herr, AFIT/ENP
U	U	U	UU	91	19b. TELEPHONE NUMBER *(include area code)* (937) 255-3636 x4524; nicholas.herr.1@us.af.mil